

**A Study on the Interactions between Water Droplets
and Solid Targets to Understand Water Droplet
Erosion**

Ming Jing

A Thesis

in

The Department

of

Mechanical and Industrial Engineering

Presented in Partial Fulfillment of Requirements

for the Degree of the Master of Applied Science (Mechanical Engineering) at

Concordia University Montreal, Quebec, Canada

April 2021

© Ming Jing, 2021

CONCORDIA UNIVERSITY

School of Graduate Studies

This is to certify that the thesis prepared

By: Ming Jing

Entitled: A Study on the Interactions between Water Droplets and Solid Targets to Understand
Water Droplet Erosion

and submitted in partial fulfillment of the requirements for the degree of

Master of Applied Science (Mechanical Engineering)

complies with the regulations of the University and meets the accepted standards with respect to originality and quality.

Signed by the final Examining Committee:

_____	Chair
Dr. Charles Basenga Kiyanda	
_____	Examiner
Dr. Charles Basenga Kiyanda	
_____	Examiner
Dr. Pantcho Stoyanov	
_____	Supervisor
Dr. Mamoun Medraj	

Approved by _____ Graduate Program Director

Dr. Sivakumar Narayanswamy

04/16/2021
Month/Day/Year

Dr. Mourad Debbabi
Dean, Gina Cody school of Engineering and Computer Science

Abstract

A Study on the Interactions between Water Droplets and Solid Targets to Understand Water Droplet Erosion

Ming Jing

Water droplet erosion (WDE) has always been a serious issue in the power generation industry. WDE is the continuous loss of material from a solid surface due to the accumulated impacts by water droplets. In gas turbines, ultra-fine droplets are purposely sprayed into the incoming air of the compressor in order to decrease the ambient temperature and increase the efficiency of the turbine. Unfortunately, this process involving water droplets, severely damages the leading edge of the compressor blades. Erosion, such as WDE, is not constant with time. It has been classified into early stages and advanced stages. Most studies on erosion have primarily focused on the early stages of erosion. Very few researchers focused on water droplets and solid interactions at the early stages of erosion, which is important in understanding WDE damage. Knowing where and how the droplets impact the target can contribute to understanding the WDE phenomenon further and propose a way to reduce WDE or even find a potential solution for WDE altogether. The purpose of our work is to explore several approaches in understanding this interaction.

One part of this work will study the effects of airflow on the trajectories of water droplets with the use of ink coated samples and computational fluid dynamics (CFD) simulation.

A secondary part will investigate and compare how different solid target samples react to the impact of water droplets. The selection of samples is as follows: flat (as-received unaltered material), grooved, and metallic foam. The grooved and metallic foam samples are employed in this work in order to stabilize a water film and dissipate the energy caused by multiple droplets impacts. The erosion tests were conducted in a rotating disc rig in accordance to the ASTM-G73 standard. The size of the droplets was 460 μm and the impact speeds were set to 150 m/s, 200 m/s, and 250 m/s. Ti-6Al-4V alloy was chosen as a sample material because it is typically used in turbine compressor blades.

During the WDE tests, it was observed that the airflow had a significant influence to drift the water streak away from the rotation center. Moreover, it can affect the trajectories and the impact position of the droplets. The airflow causes the upper half of the sample to erode faster than the bottom half. This was obvious upon observing the eroded samples after WDE tests. Furthermore, the formation and distribution of secondary droplets after the initial impact could also be influenced by the airflow within the rig. This is attributable to the lower mass of the secondary smaller droplets that are easily affected by the airflow.

Metal samples having grooves of either 0.5 mm or 1 mm depth were employed in this work along with other samples having blocked grooves to prevent water flowing downward. Incubation period and maximum erosion rate are the two main erosion resistance parameters of interest in this research. The results showed that the 0.5 mm groove had a longer incubation period than the reference sample. It also fared better than the 1 mm and bottom blocked grooved samples. This was studied by CFD simulation and is concluded as the influence of water film formation in the groove by dampening the impacts of subsequent water droplets. The 0.5 mm groove had a more suitable airflow environment to stabilize the water film in the groove than the

1 mm groove. However, at the maximum erosion rate stage, the reference sample and both sizes of grooves showed similar erosion behavior. This indicates that the maximum erosion rate stage is not affected significantly by introducing grooves and the formation of water films in them.

Porous and polyurethane-blocked samples were used as both test and reference samples respectively in the current work. Their purpose is to stabilize the water film, dissipate the impact energy, and study the interactions between water droplets and porous structure further. The results show that the porous structure can dissipate more impact energy than the solid substrate and mitigate the WDE damage to some extent.

Acknowledgements

I would like to express my sincere gratitude and appreciation to my thesis supervisor Dr. Mamoun Medraj for his time, suggestions, support, and encouragements during my MASc project at Concordia University.

I would also like to give many thanks to Dr. Abdullahi Gujba for his suggestions on my project and his help with my thesis corrections during my MASc program. My sincere thanks go to all the TMG group members, especially WDE group members Rizwan Ahmed, and Elhadi Ibrahim for their suggestions during my research. Sincere thanks will also go to Alain Belso for his help on my thesis revision and linguistic correction. Thanks, Mr. Yan Jing, for his help with my CFD simulation section. I would also like to thank Mazen Samara for his help and support throughout my experimental work. Thanks to my friends for their support during my MASc project.

Finally, I gratefully acknowledge my family. Without their endless encouragement and support, I could not have done it. You have always led by example to educate me to be a better person and encourage me to pursue my dream! Thank you!

Table of Contents

List of Figures.....	x
List of Tables.....	xiv
Chapter 1: Introduction.....	1
1.1. Problem statement.....	1
1.2. Thesis layout.....	3
Chapter 2: Literature review.....	4
2.1. WDE.....	4
2.1.1. Causes of erosion.....	4
2.1.1.1. Water hammer pressure (impact pressure).....	4
2.1.1.2. Lateral jetting.....	8
2.1.2. Time dependence of WDE.....	11
2.1.3. Parameters influencing WDE results.....	14
2.1.3.1. Impact velocity.....	15
2.1.3.2. Surface roughness.....	16
2.1.3.3. Droplet size.....	17
2.1.3.4. Impact angle.....	17
2.1.4. Splashing and secondary droplets.....	18
2.1.5. The effect of air turbulence on water droplets.....	19
2.1.6. The effect of water film formation.....	21
2.1.7. Metallic foam.....	22
2.1.8. CFD simulation in WDE.....	23
2.2. Project objectives.....	23

Chapter 3: Experimental methodology	25
3.1. Sample preparation	25
3.1.1. Ti-6Al-4V flat sample preparation.....	25
3.1.2. Grooved sample preparation.....	26
3.1.3. Metallic foam sample preparation.....	27
3.1.4. Surface roughness	28
3.2. Water flow pattern tracing experiment	29
3.3. Computational fluid dynamics (CFD) simulation.....	30
3.4. WDE test and experimental apparatus	31
Chapter 4: Results and Discussion.....	34
4.1. Results of surface roughness measurements	34
4.2. Water flowing pattern tracing experiment.....	34
4.3. Influence of the airflow on the water droplets using CFD simulation.....	38
4.3.1. Effect of the radial airflow	38
4.3.2. Effect of the axial airflow	40
4.3.3. Effect of the airflow on the impact angle.....	42
4.4. Understanding the water droplet interactions with 4 mm width grooved samples.....	43
4.4.1. WDE tests	43
4.4.2. Simulation of water droplet interactions with the grooved samples.....	46
4.4.3. WDE tests with the bottom-blocked groove sample.....	48
4.5. Understanding the water droplet interactions with the metallic foam filled groove sample.....	51
4.5.1. WDE tests	51

4.5.2. Simulation of impacting pressure on the metallic foam	52
Chapter 5: Conclusions, Contributions and Recommendations	56
5.1. Conclusions.....	56
5.2. Contributions.....	57
5.3. Recommendations and future work	58
References.....	59

List of Figures

Figure 1-1 Gas turbine engine showing compressor blades before and after erosion damage. Courtesy of MSD Coatings Technologies Co. [6].....	2
Figure 1-2 Eroded ex-service turbine blade [9]	3
Figure 2-1 Initial stage of an impact droplet, according to Heymann [16].....	6
Figure 2-2 The density contours for droplet impact with a solid wall. The impact Mach number is 0.2, the target compliance is 0.04. The labels indicate S: Shock Wave, R: Reflected, F: Focus and J: Jetting [20].....	7
Figure 2-3 After shock wave has overtaken the contact edge allowing decompression and jetting [21].....	8
Figure 2-4 a) A water droplet sends out the lateral jetting b) repeated water droplet impacts, the asperity initiates a crack c) water jetting open the crack up [22].....	9
Figure 2-5 Radial outflow velocity as a function of impact velocity [23].....	10
Figure 2-6 a) Typical erosion curve and erosion rate curve on a solid surface. The following stages have been identified thereon: (I) incubation stage; (II) acceleration stage; (III), maximum rate stage (IV) deceleration stage (V) terminal stage; [25] b) Schematic of erosion damage processes on a solid surface.....	12
Figure 2-7 Extracting the parameters from the material mass loss erosion graph.....	14
Figure 2-8 Water droplet erosion of annealed Ti-6Al-4V at impact velocity of a) 300 m/s b) 350 m/s and droplet diameter of 460 μm for the three surface conditions [9].....	16
Figure 2-9 Normalized material loss of stainless steel eroded at different impact angles [38].....	18

Figure 2-10 Flow streamlines colored by a) velocity magnitude (m/s) and b) droplet impact locations on the flat plate (Unit: m) [44].....	19
Figure 2-11 a) Computed droplet shapes (superimposed white lines) as a function of time for cases: Droplet diameter = 513 μm , and airfoil velocity = 91 m/s (left), and Droplet diameter = 388 μm , and airfoil velocity = 71 m/s (right). b) Sketch of the problem under consideration [45].....	20
Figure 2-12 Numerical analyzing of droplet impingement a) without and b) with water film [48].....	22
Figure 3-1 a) Ti-6Al-4V flat reference samples for low speed testing design b) Schematic of flat reference sample and sample holder assembling	26
Figure 3-2 a) 0.5 mm depth grooved sample b) 1 mm depth grooved sample c) Bottom-blocked grooved sample (Dimensions in mm).....	27
Figure 3-3 a) Nickel-Chromium metallic foam b) 1.7 mm depth grooved sample with metal foam filled.....	28
Figure 3-4 Oil-based ink coated samples.....	29
Figure 3-5 a) Schematic of the Water Erosion Rig b) Ti-6Al-4V flat reference samples for low speed testing design and sample holder assembly	32
Figure 3-6 Nozzles used in the experiments (a) single-ray, (b) 3-ray, and (c) multi-ray (shower-head).....	33
Figure 4-1 Ink coated samples after WDE test at 150 m/s, 200 m/s and 250 m/s	36
Figure 4-2 a) Definition of the impact angle α , D and U are, respectively, the initial diameter and the impact velocity of the primary droplet b) Effect of impact angle (D = 2.75 mm) $\alpha = 90^\circ$ U = 2.5 m/s and $\alpha = 15^\circ$ (τ : Time(s)) [59]	37

Figure 4-3 Airflow direction description figure.....	38
Figure 4-4 a) The airflow around the rotating sample and b) sample wakes at 250 m/s	39
Figure 4-5 Samples rotating in clockwise direction at 250 m/s in the test chamber showing the distribution and the magnitude of the radial sample wakes	39
Figure 4-6 Sketch of a lamella a) The velocity directions of the gas and spreading are opposite b) The velocity directions of the gas and spreading are the same.....	40
Figure 4-7 a) Side view of the simulated airflow graph b) Airflow with dividing line.....	41
Figure 4-8 Schematic for the impact angles influenced by the airflow.....	42
Figure 4-9 Simulation results of droplet impacts on the rotating sample at 250 m/s a) Initial moment b) Estimated maximum width distance of lateral jetting from the simulation.....	43
Figure 4-10 Erosion curve with different depth grooves	45
Figure 4-11 WDE test results a) reference sample (0 mm) b) 0.5 mm groove sample c) 1 mm groove	46
Figure 4-12 Water flowing mode simulation on a) flat sample b) 0.5 mm depth grooved sample c) 1 mm depth grooved samples at 250 m/s after one full rotation and prior to the next impact ..	47
Figure 4-13 Air turbulence simulation in a) 0.5 and b) 1 mm depth grooves.....	48
Figure 4-14 a) WDE test with bottom-blocked sample at 250 m/s after 40 mins b) Simulated airflow graph of the bottom-blocked sample	49
Figure 4-15 Simulation of the interactions between the impact droplets and the bottom-blocked sample a) after 1.5×10^{-6} s b) after 4.5×10^{-6} s	50
Figure 4-16 a) Initial metallic foam with polyurethane-blocked b) Metallic foam with Polyurethane-blocked, after 20 mins WDE test at 150 m/s c) initial metallic foam d) metallic foam after 20 mins WDE test at 150 m/s.....	52

Figure 4-17 Pressure drop curve for NC4753 [54] 53

Figure 4-18 Pressure monitoring chart of contact surface for a) Polyurethane-blocked metallic foam b) porous metallic foam 54

Figure 4-19 Time variation of pressure during the WDE test on a) polyurethane-blocked metallic foam b) porous metallic foam 55

List of Tables

Table 3-1: Properties of Recemat metallic foam.....	28
Table 3-2: Parameters of tested chamber conditions	30
Table 3-3: Setups for the numerical parameters in the simulations.....	31
Table 3-4: Parameters for the single ray nozzle.....	33
Table 4-1: Surface roughness of reference and tested samples.....	34
Table 4-2: The number of impingements at 150 m/s, 200 m/s, and 250 m/s within 2 seconds....	36
Table 4-3: The mass loss of reference, 0.5 mm depth groove, and 1 mm depth groove sample in the first 60 minutes of testing	46

Chapter 1: Introduction

Water droplet erosion (WDE) of gas and steam turbine blades has always been a serious problem in the power generation industry. WDE results in severe damage on the leading edge of compressor blades due to the interactions between the rotating blade and water droplets, thereby shortening the service life of the blade. This chapter states the WDE problem. The thesis layout is presented in this chapter as well.

1.1. Problem statement

In the power generation industry, gas turbines suffer from the effect of high ambient temperatures which results in the output power efficiency dropping significantly; this issue is worse in the summertime. For every 1°C ambient temperature increase, there is a 0.54-0.90% decrease in output power efficiency [1–3]. In order to increase turbine efficiency, the ambient temperature must be kept as low as possible. Different cooling methods such as fog cooling [3] or evaporative cooling [2] have been explored by industries for decades. Due to the high cooling efficiency and low cost requirements, fog cooling (where ultrafine liquid droplets are employed to cool the incoming air) has been identified as the ideal technique for mitigating this problem [4]. The ultrafine water droplets are introduced to the gas turbine at a specific pressure with an atomizing nozzle. Fogging droplets reduce the temperature of the blades directly; this makes fogging one of the most efficient and preferred ways for turbine cooling.

Although the sprayed droplets reduce the temperature and increase power output [4], the impacting water droplets cause severe erosion damage to the leading edge of the rotating compressor blades, especially at high speed [5]. This damage is termed “water droplet erosion (WDE)” or “liquid impingement erosion (LIE)”. WDE is defined as the continuous loss of material from a solid surface due to accumulated impacts by water droplets. WDE or LIE can

degrade the performance of a turbine and shorten the service life of the blades. Fig. 1-1 shows a typical gas turbine compressor blade before and after WDE damage.

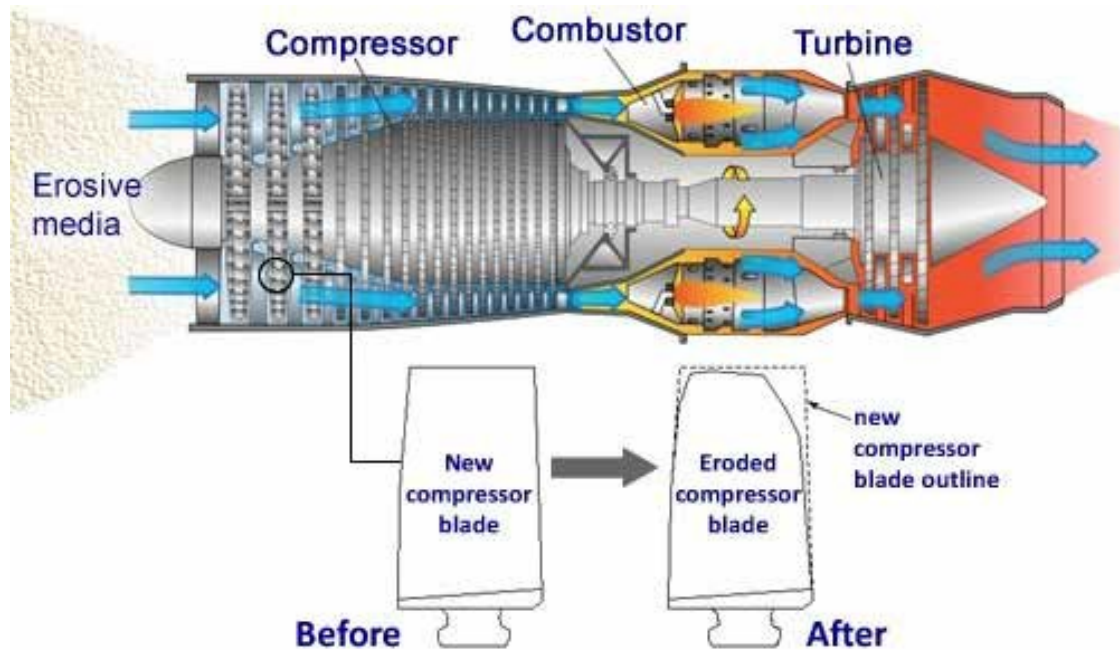


Figure 1-1 Gas turbine engine showing compressor blades before and after erosion damage.
Courtesy of MSD Coatings Technologies Co. [6].

Fig. 1-2 shows a real-life eroded compressor blade caused by WDE. WDE seriously shortens the service life of the turbine. This issue needs to be addressed to ensure the turbine keeps working at peak efficiency. Not only do damaged blades cause the turbine to run at a reduced efficiency, if the erosion continues unchecked, it can lead to catastrophic failure. To address this issue, many researchers have attempted some form of surface treatments [7, 8]; however, the enhancements were not very significant. The purpose of this work is to experimentally recreate the water droplet interactions with the impacting samples and the effects of airflow in order to understand the WDE issue further and propose a way to reduce it or even find a potential solution altogether.



Figure 1-2 Eroded ex-service turbine blade [9].

1.2. Thesis layout

This thesis is composed of five chapters. Chapter 1 states the current research problem. Chapter 2 reviews the WDE phenomenon and the causes of different erosion features are summarized at different erosion stages. The effect of some parameters such as impact speed, droplet size, etc. are introduced in this chapter. Water film and the effects of airflow on the trajectories of the water droplets are also highlighted in chapter 2. The research motivations and objectives that relate to the literature findings are also mentioned in this chapter. Chapter 3 introduces the experimental methods and set up. The parameter selections are also introduced in this chapter. Chapter 4 presents the experimental results of water droplet interactions with different solid impacting samples explained by simulation. The effects of the airflow on the droplets in the WDE test are also presented and discussed in this chapter. Lastly, Chapter 5 summarizes the conclusions and contributions of the current work. Recommendations for future research are highlighted at the end of this chapter.

Chapter 2: Literature review

The WDE behavior of Ti-6Al-4V, a common alloy used in compressor blades, will be reviewed in this chapter. Also, the causes of WDE, the parameters that influence the WDE behavior of materials, the effects of airflow on the trajectories of droplets and the influence of water film formation will be introduced in this chapter.

2.1. WDE

2.1.1. Causes of erosion

WDE is a time-dependent progressive damage [10]. WDE damage has been studied for decades. There are two main causes of WDE damage: (1) Impact pressure induced at the impacted area (water hammer pressure) [11] and (2) The radial liquid flow (lateral jetting) along the surface at high speed, which occurs after the initial droplet pressure release [12]. The two main causes are explained in the following sub-sections.

2.1.1.1. Water hammer pressure (impact pressure)

When a liquid droplet impacts a solid surface, impact pressure is generated and a shock wave is propagated simultaneously. This is the initial stage and is important in understanding WDE. In 1928, Cook [13] attempted to explain this impact pressure produced by the liquid droplets on metallic surfaces with the water hammer phenomenon and emphasized the dramatic influence of the water hammer pressure on WDE. Based on this one-dimension water hammer theory, the impact pressure can be represented in equation (1) [13]:

$$P = \rho_0 C_0 V_0 , \quad (1)$$

Where ρ_0 and C_0 are the density and the acoustic velocity of the undisturbed liquid droplets, respectively. V_0 is the impact speed. However, the velocity of the shock wave is not always equal

to the acoustic speed. In this case, when the droplet impacts at a high speed, the shock wave speed has to be treated as a function of the water hammer pressure itself.

Moreover, Heymann [14] pointed out that the one-dimension model of the water hammer did not correspond to the real condition where the shock wave pressure propagates as a dome shape in the droplets, not a plane shape, shown as Fig. 2-1. The pressure at the edge of the compressed impacted droplets can attain levels up to three times higher than the impact pressure calculated by the water hammer pressure equation (1). However, the pressure at the edge of the contact points lasts for a very short time duration and is usually negligible and ignored [15]. In 1969, a two dimension pressure equation (2) was presented by Heymann [16] to explain the case which is more representative:

$$P = \rho_0 C_0 V_0 \left[1 + k \left(\frac{V_0}{C_0} \right) \right]. \quad (2)$$

Here, k is a constant for a specific liquid, and $k = 2$ is for water. The schematic of an impact droplet on a rigid solid surface can be seen in Fig. 2-1. The liquid behind the shock wave envelope line is compressed and the rigid surface underneath this area has a high pressure which is responsible for the initial cracks on the solid after repetitive impacts. In 1981, Lesser [17] discussed Heymann's work [16] and expanded it significantly. He calculated the detailed edge pressure for both two-dimensional and three-dimensional spherical droplets and found that in these two cases, the edge pressure only depends on the impact speed and the instantaneous angle between the liquid and the solid at the moment when the droplet impacts the surface. Hence, he suggested that the two-dimensional droplet impact model can be applied to study the early stage of the droplet impact instead of three-dimensional droplet impact model. Furthermore, he also proposed that the pressure of cylindrical droplets is higher than spherical droplets, but the edge pressure is identical for both cases. In general, there is consistency between Heyman's work [16]

and other researchers such as Lesser [17]; however, this was in disagreement with other researchers such as [18, 19]. For instance, in 1955, Engel [19] proposed another two-dimensional pressure equation:

$$P = \frac{1}{2} \alpha \rho_l C_l V_i, \quad (3)$$

where α approaches unity for the high-speed impact and $\frac{1}{2}$ is the consequence of a spherical liquid droplet, ρ_l is the density of the liquid, C_l is the speed of sound in the liquid, and V_i is the impact speed of the liquid droplet.

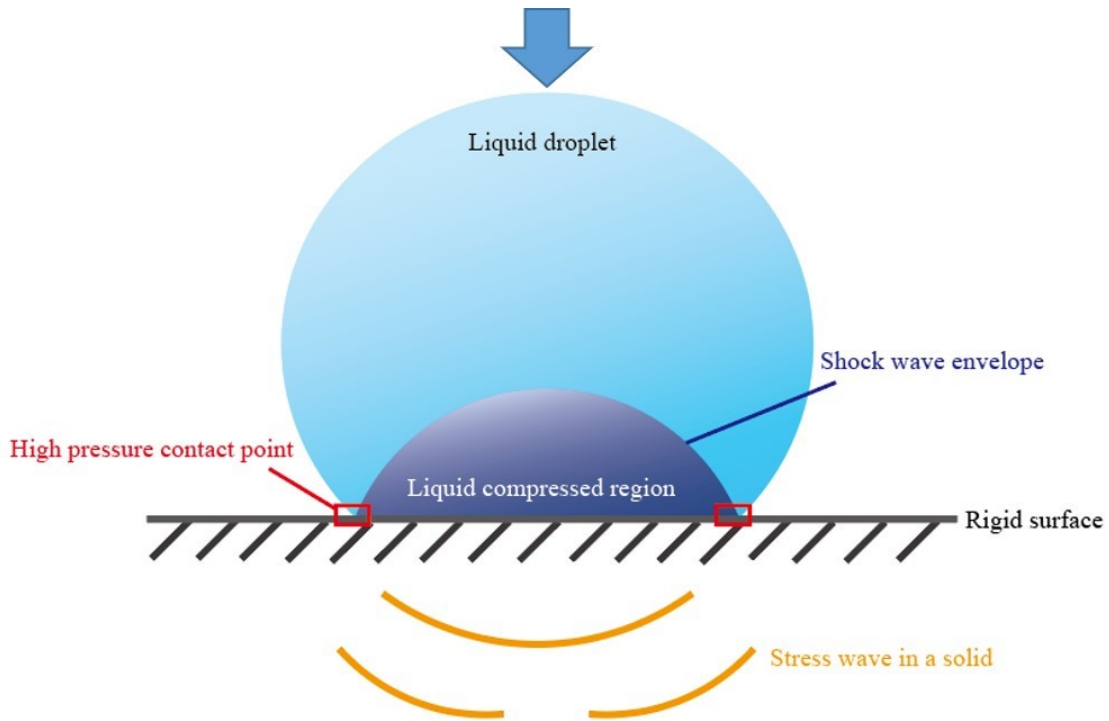


Figure 2-1 Initial stage of an impact droplet, according to Heymann [16].

Accordingly, Sanada et al. [20] applied Heymann's pressure equation and numerically studied the shock wave pressure propagation in two dimensions. Fig. 2-2 presents the shock wave propagation in a compressed water droplet. The liquid droplet impacts a ductile target with an impact speed of Mach 0.2. A shock wave (S) is generated after the droplet impacts the solid

surface. The shock wave proceeds to expand along the shock wave envelope line in the compressed liquid droplet. A low pressure is generated after the reflection (R) of the shock wave envelope on the top of the droplet. Finally, the shock wave focuses on one point (F) shown in Fig. 2-2 (e), and at the bottom edge of the compressed droplet, lateral jetting (J) commences, as shown in Fig. 2-2 (f). After the repetitive impacts of the droplets, the rigid surface sample begins to initiate damage from the high pressure.

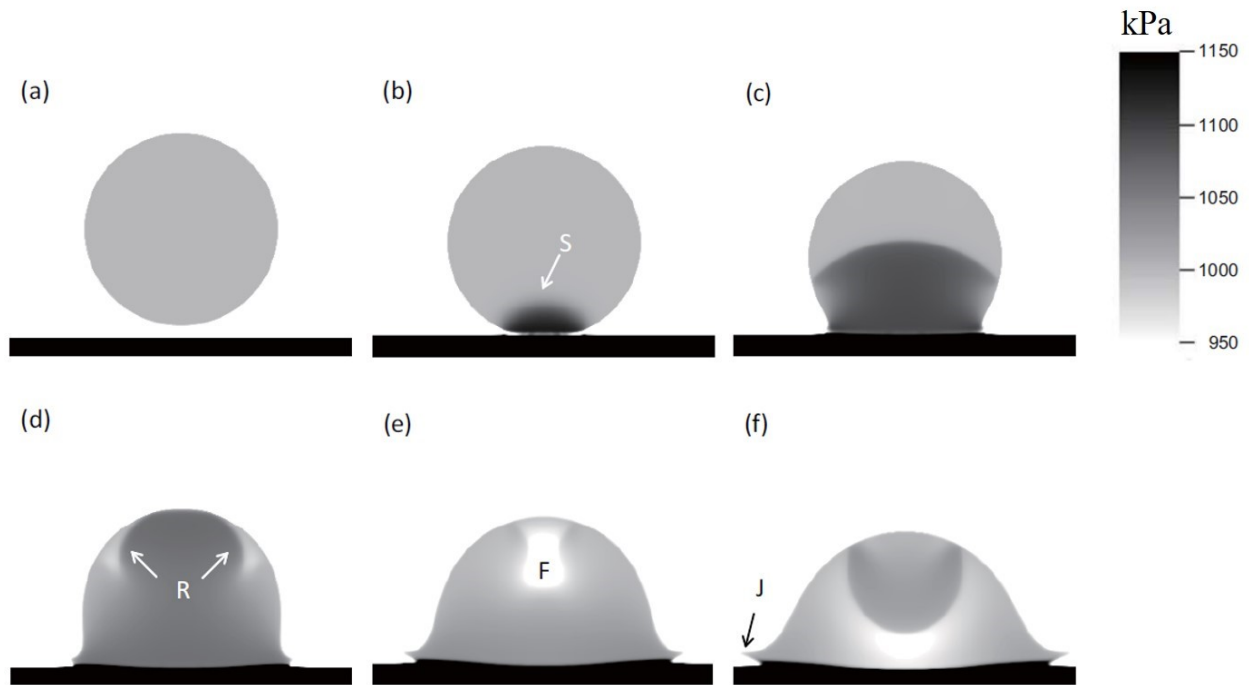


Figure 2-2 The density contours for droplet impact with a solid wall. The impact Mach number is 0.2, the target compliance is 0.04. The labels indicate S: Shock Wave, R: Reflected, F: Focus and J: Jetting [20].

Since the high impact pressure of the water droplets is one of the main causes of the initial damage, the contact pressure between the droplets and the solid surface at impact is paramount in order to predict the WDE damage. The higher the contact pressure, the faster the erosion damage. In this work, the value of contact surface pressure is used to estimate the length

of the incubation period of the porous metallic foam and polyurethane-blocked metallic foam in the CFD simulation.

2.1.1.2. Lateral jetting

Since there is no free surface between the liquid droplet and the surface at impact, the high pressure inside the compressed liquid needs to be released. When the shockwave overtakes the contact edge, a free surface is generated and releases the pressure within the high pressure region of the compressed droplet [21]. Hence, the lateral jetting (radial outflow) occurs due to the pressure release [21]. The jetting process is shown in Fig. 2-3.

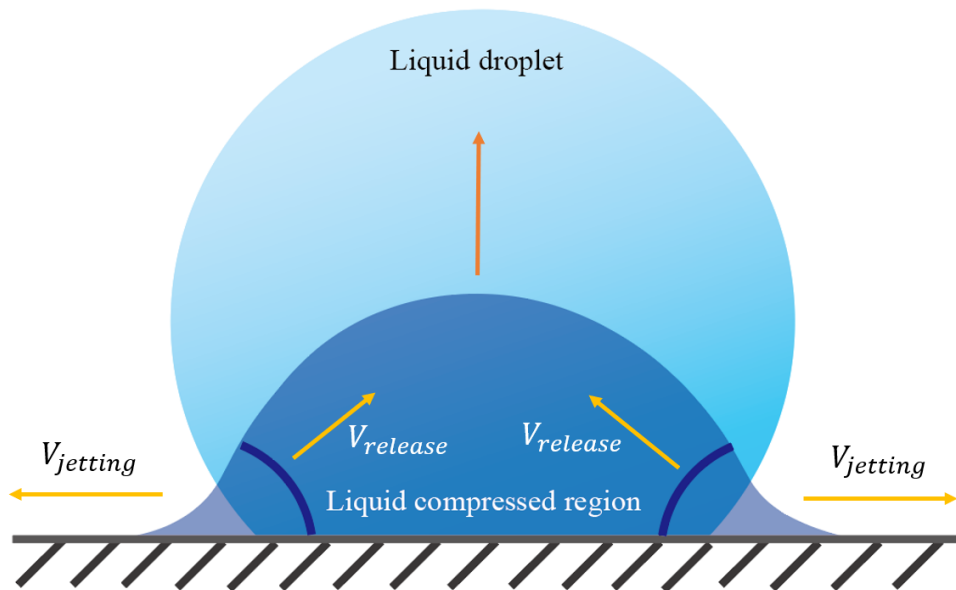


Figure 2-3 After shock wave has overtaken the contact edge, allowing decompression and jetting [21].

In the 1970s, Heymann [22] proposed a theory on how lateral jetting damages the surface of a solid with repetitive water droplet impacts by explaining the mechanism of lateral jetting. Lateral jetting interacts with surface irregularities, then damages the base material [22] as shown in Fig. 2-4. When high pressure release starts, the lateral jetting begins to spread across the surface of the material.

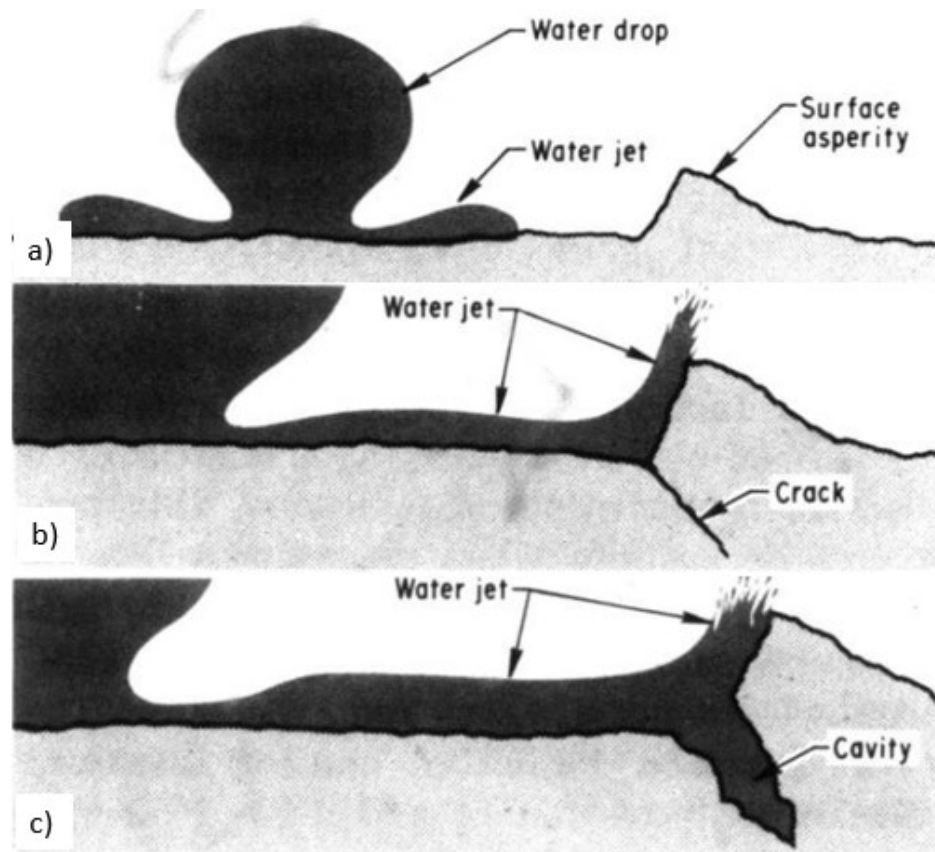


Figure 2-4 a) A water droplet sends out the lateral jetting b) repeated water droplet impacts, the asperity initiates a crack c) water jetting open the crack up [22].

With the repetitive impingements of the lateral jetting on the wall of asperity, the initial cracks develop at the base of the asperity surface and are opened up by the continuous lateral jetting. This lateral jetting acts on the initial depressions that were created by repetitive impingements and results in the erosion pits nucleation. Eventually, the hydraulic penetration mechanism accelerates the expansion of these pits and initial erosion craters, which results in the removal of material.

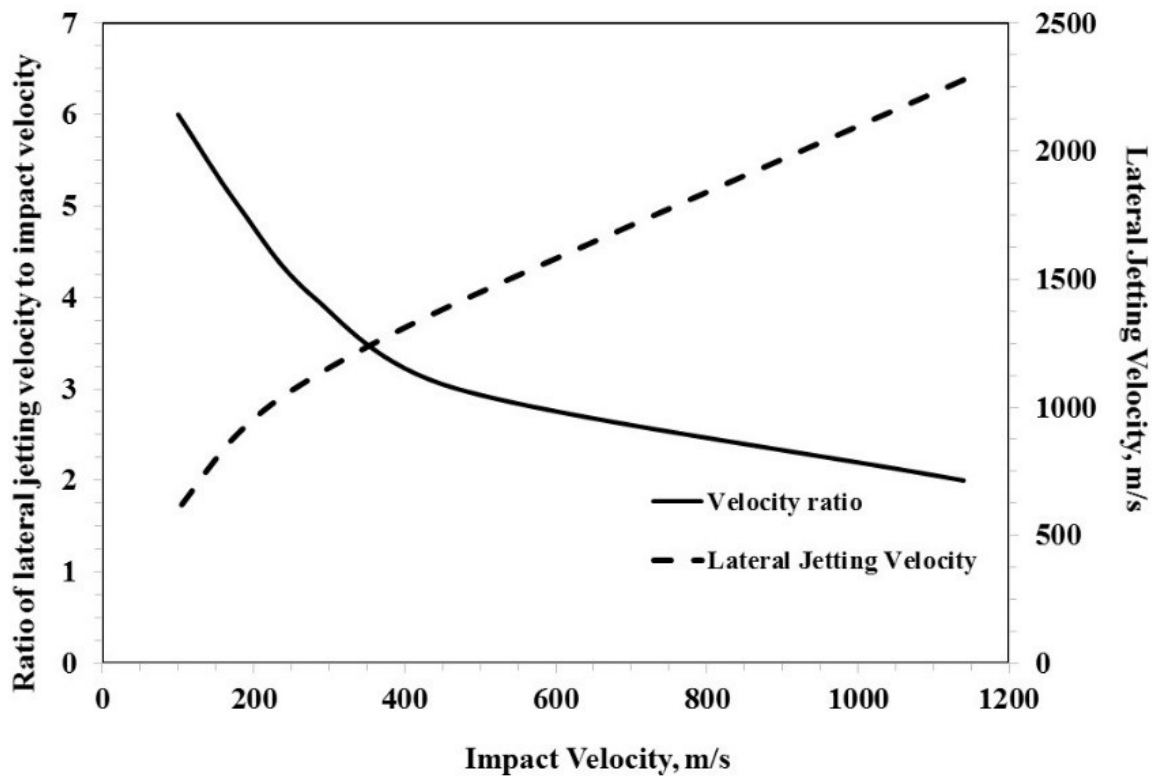


Figure 2-5 Radial outflow velocity as a function of impact velocity [23].

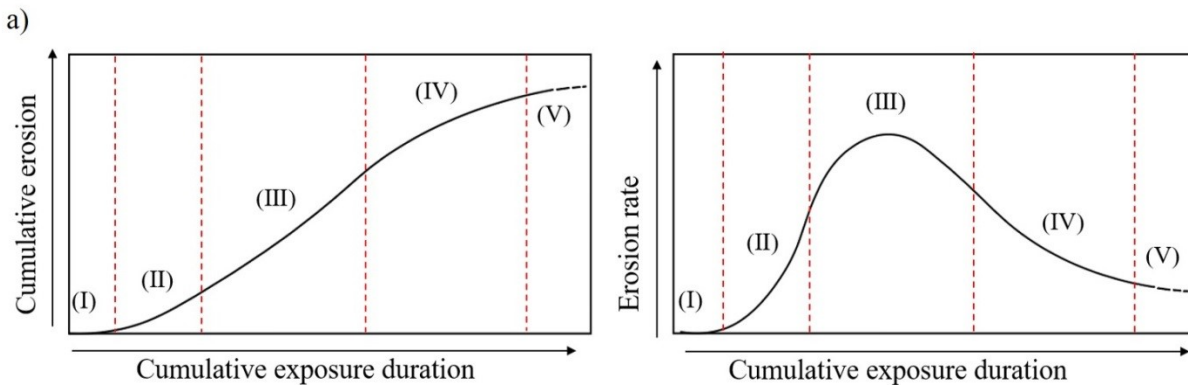
In this work, the lateral jetting spreads the water out to form a film. This water film is expected to dampen the impact energy before the irregularities and craters form. However, when the craters begin to occur, the lateral jetting contributes to expanding the craters. At this point, the effect of the water film would be diminished. Thus, in this work, studying the lateral jetting pattern before craters appear is important to understand the effect of the water film and the interactions of the water droplets with the impacting targets.

Furthermore, the lateral jetting is able to reach speeds several times higher than the impact speed. The relationship between the lateral jetting and the impact speed has been proposed by Jekins and Booker [23] as demonstrated in Fig. 2-5. For instance, when the impact

speed is around 200 m/s, the lateral jetting attains a speed of 1100 m/s approximately. This is around 5 times faster than the impact speed. Thus, in this work, the impact speed of 250 m/s is used in order to avoid the water film disappearing too fast from the surface yet to be as close as possible to the typical impact speeds found in common gas turbines running at average working conditions (e.g. 350 m/s is an average rotating speed for a gas turbine compressor [24]).

2.1.2. Time dependence of WDE

In 1967, Heymann [25] stated that the material mass loss of WDE does not change linearly with time. He found that during the WDE tests, the material goes through five stages, as demonstrated in Fig. 2-6 (a). The different erosion stages have been separated by red dashed lines. Field et al. [26] summarized the features of the erosion damage on a ductile solid surface. The material removal mechanism in different erosion stages in Fig. 2-6 (b) corresponds to the erosion curves in Fig. 2-6 (a). The definition of the stages is presented as follows:



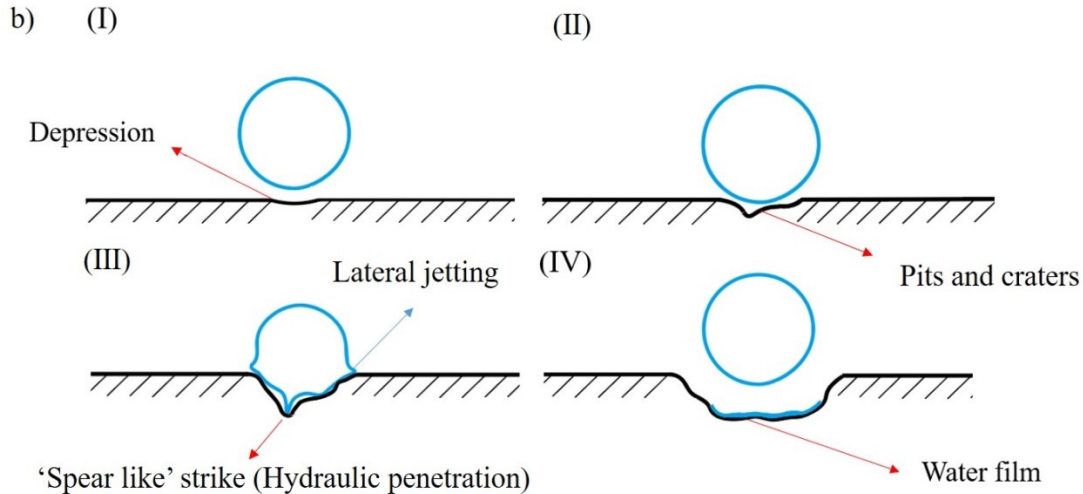


Figure 2-6 a) Typical erosion curve and erosion rate curve on a solid surface. The following stages have been identified thereon: (I) incubation stage; (II) acceleration stage; (III), maximum rate stage (IV) deceleration stage (V) terminal stage; [25] b) Schematic of erosion damage processes on a solid surface.

(I) Incubation stage: In this stage, droplets mainly cause depressions that are not easily observed on the surface. This period is presented in the Figs. 2-6 (a) (I) and (b) (I). Furthermore, there is either no or negligible mass loss at this stage. Various testing conditions of the WDE can influence the duration length of this stage. For instance, a higher impact velocity or a rougher surface condition can reduce the duration of this stage.

(II) Acceleration stage: In this period, the weight loss increases due to the repetitive droplet impacts. The pits and cracks can be observed on the surface and is visually represented in Fig. 2-6 (b) (II). This period is found in the schematic in Fig. 2-6 (a) (II).

(III) Maximum erosion rate stage: In this period, the erosion rate reaches and maintains the maximum value. The cracks become deeper and wider because of the influence of the lateral jetting and hydraulic penetration damage; it is shown in Fig. 2-6 (a) (III).

(IV) Deceleration stage: Once the craters reach a certain depth and width, the erosion rate decreases. One of the early attempts to explain the decrease in erosion rate at this stage was done

by Honegger [27]. He proposed a theory that when the crater reaches a certain depth, a layer of liquid film forms. This film dampens the impact energy from subsequent water droplets. The hypothesis proposed by Honegger is illustrated in Fig. 2-6 (a) (IV) and this corresponds to the deceleration stage in Fig. 2-6 (b) (IV). The energy from the successive impacting droplets is absorbed by the water trapped in the crater. Heymann [25] also mentioned that when the erosion enters the deceleration stage, the water remaining in the pits and craters plays a role of a cushion and helps to protect the surface. This indicates that a water film may become one of the possible solutions to mitigate WDE. Thus, we will study and discuss the effect of a water film on mitigating WDE in this work.

(V) Terminal stage: This is the last stage of the WDE erosion. The erosion rate comes back to a constant value that fluctuates up and down irregularly. Usually, this stage is not widely studied.

Mass loss versus exposure time is usually reported according to ASTM G-73-10 [28]. In addition, for the purpose of deriving certain parameters such as erosion rate, the mass loss of the material versus the exposure time is used for the erosion curve. Three important lines can be extracted from the actual test curve. These lines define the significant parameters shown in Fig. 2-7. The first line defines the length of the incubation period and is presented as (A) in Fig. 2-7. The second line is extracted by fitting the best line through the data points in the maximum erosion rate stage. The slope of this line (B) presents the maximum erosion rate. In this thesis, these two parameters (incubation period length and maximum erosion rate) are the most important parameters and represent the erosion performance. The third line is defined to describe the terminal erosion rate (C).

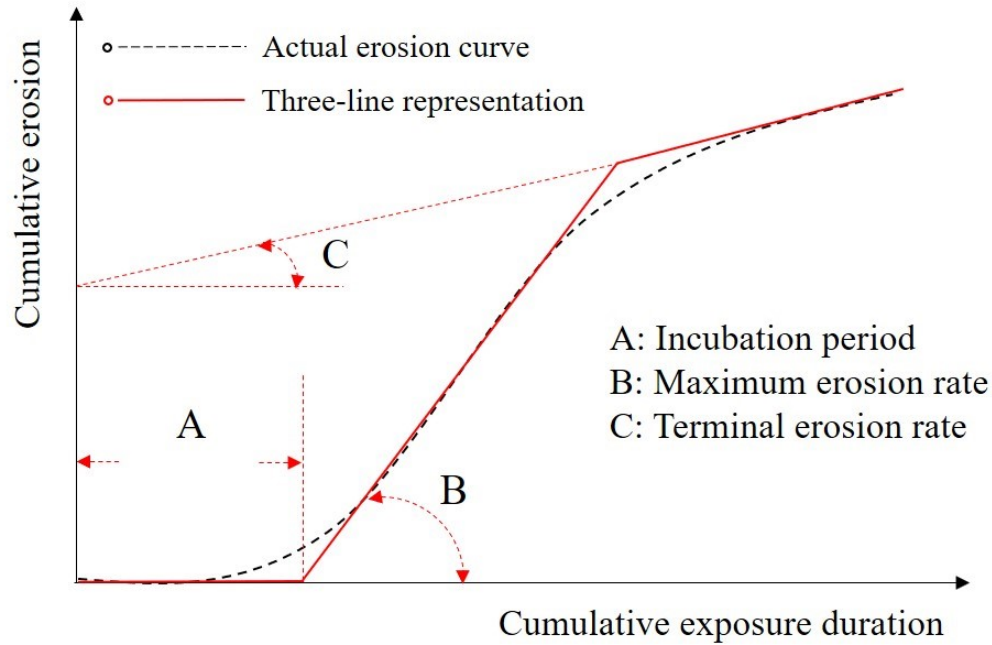


Figure 2-7 Extracting the parameters from the material mass loss erosion graph.

In summary, the erosion graph in this work will be plotted according to the actual experimental data. Furthermore, the three-line representation method will be used to analyze the data in this work. However, the third line will not be utilized. In the erosion of solid materials, mass loss has large fluctuations that are present in the terminal erosion stage. Since the present work studies the interactions between the water droplets and the solid impacting sample, it is more important to study the incubation and maximum erosion rate stages.

2.1.3. Parameters influencing WDE results

As one of the most complex erosion phenomena in the gas turbine industry, WDE could be influenced by many parameters such as impact speed, water droplet size, and impact angles [10, 11]. Studying these parameters is important for understanding the WDE behavior of materials.

2.1.3.1. Impact velocity

Impact velocity is one of the most important parameters that influences erosion behavior. In 1967, Heymann [29] proposed several important empirical relationships between the droplet's impact velocity and the erosion rate based on fitting the experimental data from the literature; amongst which, the most important three equations are presented as follows:

$$E = a V^n , \quad (4)$$

where E is the erosion rate and V is the impact velocity. Constant number a and impact speed exponent n depend on the test conditions. This is the most commonly used equation for presenting the relationship between the impact velocity and the erosion rate. However, this simple relationship implies that the erosion happens to the materials no matter how low the impact velocity is. Obviously, it is not always the case since the incubation period exists. In the case of severe situations, where the impact velocity is very high, there would be no incubation period present in the erosion graph [25]. Thus, Equation (4) could be applied. When the incubation period is present in the erosion graph, a more general equation is proposed [25]:

$$E = a(V - V_c)^2 , \quad (5)$$

where V_c is a critical or threshold velocity below which the erosion is negligible. This can reflect the incubation period in the erosion graph. According to [29], it is not as accurate as equation (4) within the range of impact velocity ($1.5 < \frac{V}{V_c} < 3$). Another equation [29] is proposed based on an analogy to fatigue:

$$E = a e^{nV} . \quad (6)$$

In this equation, when the erosion rate $E \rightarrow 0$, $V = V_c$. However, this equation was not referred to in most literatures compared to equations (4) and (5) [29].

It could be concluded from the above three equations that the velocity exponent is important for presenting the relationship between the erosion rate and the impact velocity. It is presented by many researchers and also depends on other parameters [30, 31], such as liquid droplet size and tested materials. In this work, erosion rate is one of the most important parameters to evaluate the effect of the water film after the craters occur.

2.1.3.2. Surface roughness

It has been reported that surface roughness is related to the incubation time and the erosion rate of materials. For instance, Kirols et al. [9] studied the effect of initial surface roughness on the WDE behavior of Ti-6Al-4V. Samples with average initial surface roughness values (R_a) of $0.3 \mu\text{m}$, $0.12 \mu\text{m}$ and $0.04 \mu\text{m}$ were employed in their experiments. Tests were performed with an average droplet size of $460 \mu\text{m}$ at 300 m/s and 350 m/s . Experimental results are shown in Fig. 2-8.

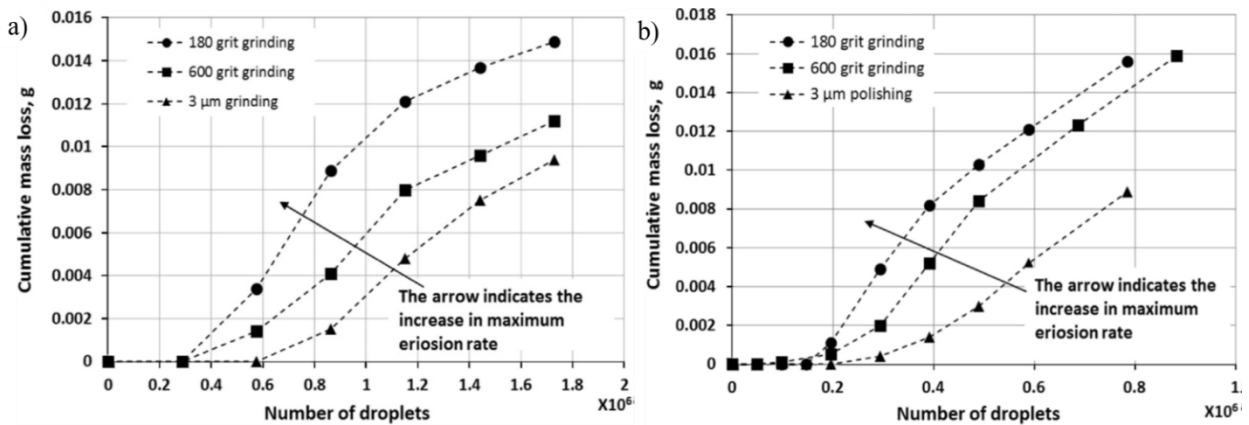


Figure 2-8 Water droplet erosion of annealed Ti-6Al-4V at impact velocity of a) 300 m/s b) 350 m/s and droplet diameter of $460 \mu\text{m}$ for the three surface conditions [9].

It can be seen from Fig. 2-8 that the incubation period is reduced and the erosion rate is increased when the tested samples have higher surface roughness values. Although more experiments involving a wider range of impacting speeds need to be performed to help better

understand the influence of the surface roughness, the work of Kirols et al. [9] emphasizes that surface roughness needs to be monitored during the WDE studies. In this work, the reference and the test samples have similar surface roughness.

2.1.3.3. Droplet size

The effect of water droplet size has been investigated by several researchers [32–34]. Among them, Alder [34] found that a droplet with a larger radius of curvature causes more damage on the sample when the test speed is the same. Das et al. [35] simulated the effect of water droplets characteristics on a fan rotor and they found that droplet size had a significant effect on the trajectories of droplets. A droplet with a larger diameter (larger mass and enhanced inertia) was rarely influenced by the airflow produced during the test; it tended to have a straighter droplet trajectory [36]. On the contrary, a smaller droplet with less mass (the secondary droplet for example) had a tendency to follow the airflow streamline and might not impact the rotating sample. The droplets of 460 μm diameter are used in this work. The reasons of using this droplet size is because the nozzle size used in this work is 400 μm and the droplet distribution of which has been reported in [11, 37]. It has been found that the 400 μm orifice of the nozzle generated a droplet size with an average of 460 μm . Furthermore, a smaller droplet size is vulnerable to evaporation in the rig due to vacuum pressure.

2.1.3.4. Impact angle

As one of the influencing parameters of WDE, the impact angle had also been studied by some researchers [32, 33, 38]. Among them, Ahmad et al. [38] reported that a 90-degree angle causes the most severe WDE damage. The volume loss after 50 hrs at different degrees has been shown in Fig. 2-9. It can be seen from Fig. 2-9 that the impact angle is a negligible influencing

parameter as it is around 90 degrees in this work and the angle change is not significant. In this work, the effects of the airflow on the impact angle are investigated.

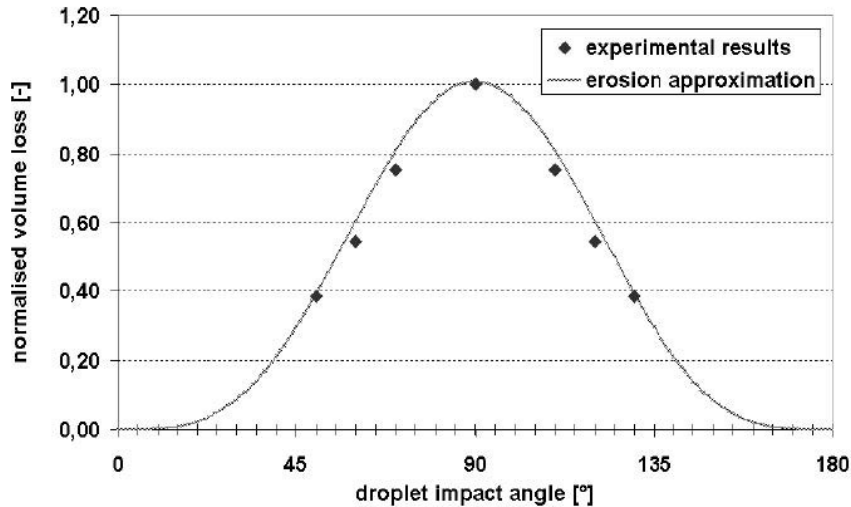


Figure 2-9 Normalized material loss of stainless steel eroded at different impact angles [38].

2.1.4. Splashing and secondary droplets

When a droplet impacts a solid surface at a high velocity, a lamella forms at the end of the lateral jetting stage. The mechanism of splashing is a result of instability of the spreading lamella [39]. When the lamella detaches from the solid surface, the lamella shatters into two or more secondary droplets [39]. This process is called splashing. However, other theories may also contribute to the splashing mechanism. For instance, the compressibility of the impacted liquid droplets in the first stage [40], the cavitations within the impacted droplets [41], and the temperature of the solid surface [42] might also contribute to splashing.

Normally, secondary droplets are not the main reason that causes erosion. Because these smaller droplets have less mass than the initial droplets, they create less impact pressure. Secondary droplet formation depends on the splashing threshold conditions [40]. The splashing threshold is believed to relate to the properties of the surface and impact droplets such as, surface

tension, surface roughness, viscosity of the liquid and the radius of droplets [39, 43]. In this work, the causes of splashing and the splashing patterns will be studied and discussed.

2.1.5. The effect of air turbulence on water droplets

Herring et al. [44] simulated the influence of the air turbulence on the water droplet impingements on flat samples. The simulation was performed at very low speed (75 m/s) and at atmospheric pressure, which is more relevant to wind turbine applications. As the samples rotate, air turbulence is produced. Fig. 2-10 (a) presents the simulated sample wakes graph. They proposed that the trajectory of the falling droplet is influenced by the passage of the previous sample rotation. The droplet impact path moves radially outward from the center of the droplet release position [44], shown in Fig. 2-10 (b). The sample rotating direction in the simulation is counter-clockwise and the rotation center is on the right of the picture, seen in Fig. 2-10 (a) and (b). The work of Herring et al. [44] used multiple nozzles and single droplet model to perform the simulation; however, the current work is focused on multiple droplet impacts generated by a single nozzle.

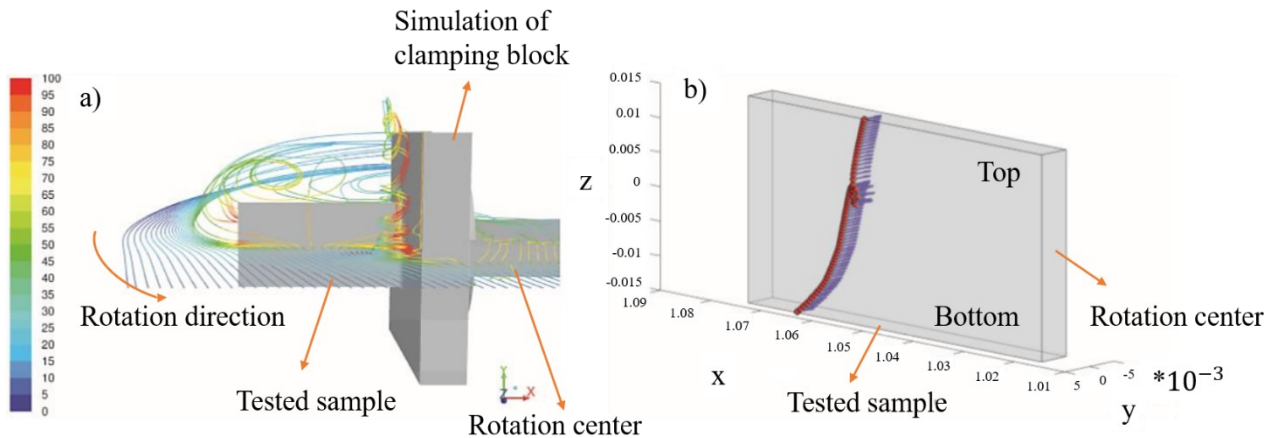


Figure 2-10 Flow streamlines colored by a) velocity magnitude (m/s) and b) droplets impact locations on the flat plate (Unit: m) [44].

Sor et al. [45] reported a model to predict the trajectories of water droplet with airfoil samples during WDE tests. They assumed that the droplet deforms along the vertical direction and the sample's wake only influence the trajectories of the droplets horizontally. The vertical component of the sample's wake is negligible and therefore ignored. The computed droplet trajectories are shown in Fig. 2-11 (a). The droplets are released freely from the droplet generator. The incoming airflow in Fig. 2-11 (b) is caused by the rotating sample wakes. The computed trajectories of the droplets are in agreement with the simulation of Herring et al. [44]. This indicates that the airflow might be one of the factors which can affect the trajectories of the droplets in this work.

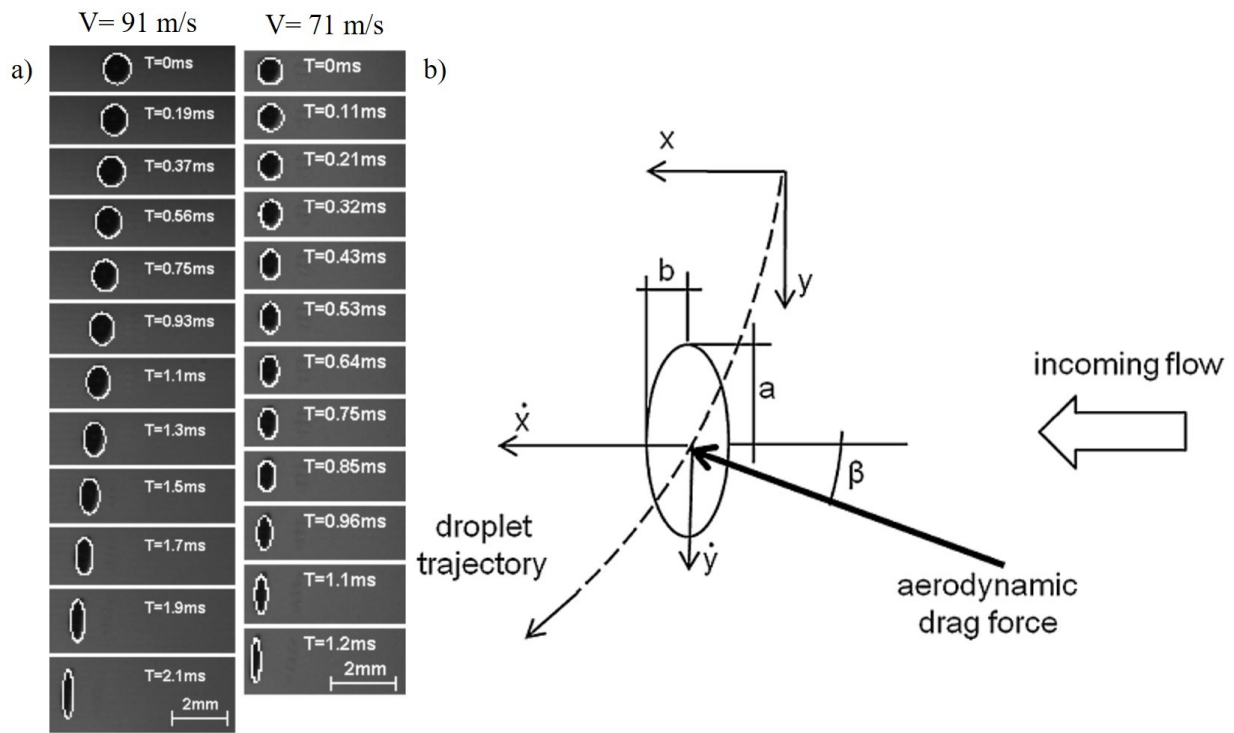


Figure 2-11 a) Computed droplet shapes (superimposed white lines) as a function of time for cases: Droplet diameter = $513 \mu\text{m}$, and airfoil velocity = 91 m/s (left), and Droplet diameter = $388 \mu\text{m}$, and airfoil velocity = 71 m/s (right). b) Sketch of the problem under consideration [45].

Therefore, in this work, the effects of the airflow are studied at a high speed (250 m/s) in a vacuum (50 mbar) chamber by experimentation and by simulation in order to help understand the interactions between the water droplets and the solid impacting sample.

2.1.6. The effect of water film formation

Most of the current research focuses on using various surface treatments to explore an effective way to mitigate the WDE problem such as laser peening [7] and deep rolling [8]. However, these surface treatments have not shown any significant enhancements. A water film has been found to mitigate the damage caused by WDE and provides a potential method to reduce or eliminate WDE.

In the 1960s, Brunton et al. [46] found that when a high speed liquid droplet collides with a wetted solid surface, the deformation of the impingement is mitigated on an aluminum plate. Furthermore, he pointed out that as the water layer thickness increases on the surface, the contact pressure of the center impacting area can be reduced by 50% compared to the dry solid surface. However, Shi [47] reported that in some cases, the water layer trapped in previously formed pits can be forced into cracks and cause further damage.

Most recently, Fujisawa et al. [48] reported numerical and experimental studies showing that the impact stress is significantly reduced by a water film when the tests are performed in a static apparatus, as shown in Fig. 2-12. The base material under the water film suffers less impact energy compared with the dry surface. In another work, Fujisawa [49] also reported that when a “V” groove sample is impacted by droplets, the water film in the groove can diminish part of the impact energy and is related to the ratio of the groove depth to the diameter of the water droplets. This indicates that when the same average droplet size impinges grooves with different depths, the WDE performances might be different. Furthermore, Sasaki [50] and Xiong

et al. [51] studied the impact of water droplets on the dry and wet surfaces using numerical modeling. A similar result in their work concluded that a water film can decrease the impact energy and indicates that a water film may provide valuable insight in terms of WDE mitigation. However, no researcher has studied the performance of a water film in conjunction with a dynamic rotating disc rig. In this work, multiple samples were designed with different geometries in order to stabilize a water film and study the effect of the water film formation during the WDE tests. Each of these samples will be studied and discussed in Chapter 4.

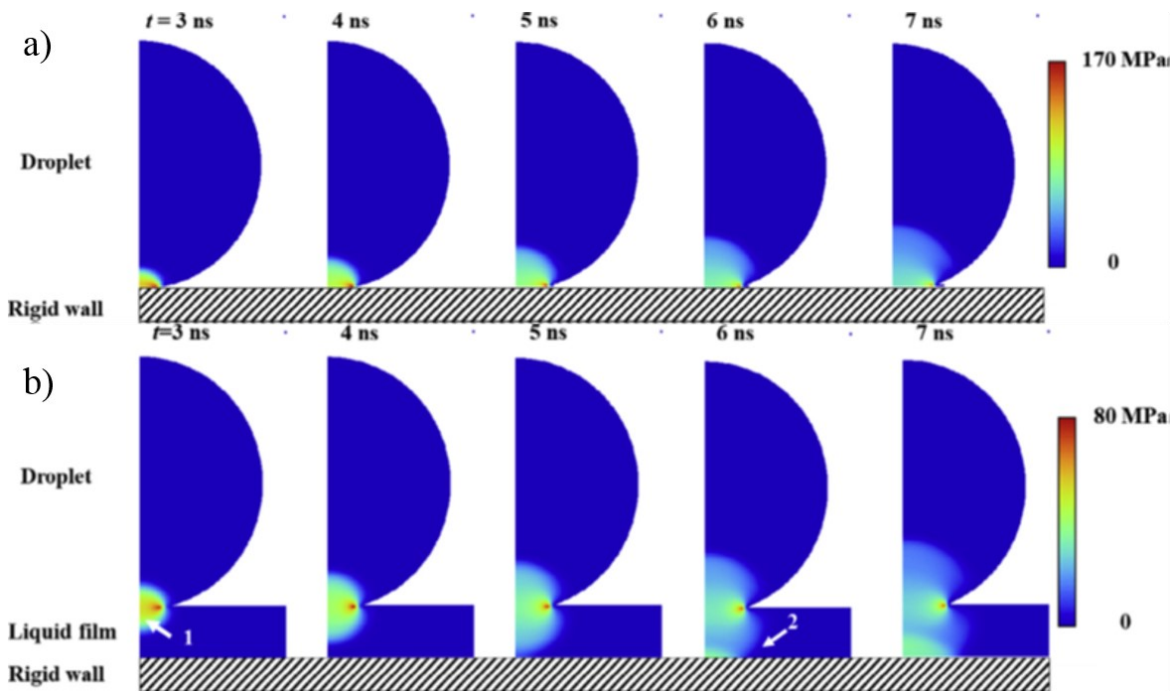


Figure 2-12 Numerical analysis of droplet impingement a) without and b) with water film [48].

2.1.7. Metallic foam

The term “metallic foam” is used to describe a metallic material that has voids. “Cellular metal”, “porous metal” and “metal sponge” are also terms used to describe these types of metallic materials [52]. Banhart [53] defined foams as uniform dispersions of gas in either liquid or solid. Thus, the capability of gas to pass through the foams is a significant parameter for the

applications of the foams. This capability is related to the magnitude of “pressure drop” taking place through the metal foam.

Usually, metallic foam has a large range of applications for any given problem depending on factors such as morphology, metallurgy, processing, and economy [54]. So far, a material with a porous structure such as metallic foam, has not been studied for understanding WDE.

2.1.8. CFD simulation in WDE

The effects of airflow on the droplets and their trajectories have been investigated by others researchers [35, 45, 55] using computational fluid dynamics (CFD) simulation. However, the impact velocity used in their experiments were quite low compared to the actual speeds found in gas turbines. Furthermore, no one has reported on how the airflow affects the water droplet interactions with the solid material. Hence, in this work, CFD simulation is employed to analyze and understand the experimental observations from the WDE tests.

2.2. Research objectives

The present study focuses on the investigation of water droplet interactions with the impacting solid material. Since the trajectories of the water droplets could be influenced by the airflow produced by the rotating samples, the airflow and its effects on the water droplets are also investigated in this work.

The objective of this thesis is to investigate the behavior of the water droplet interactions when impacting flat, grooved, and metallic foam filled samples experimentally and by CFD simulation. A rotating disc water erosion rig is used for the WDE tests. Ansys Fluent (Ansys Inc., USA) is employed for the simulation of the airflow turbulence and the interactions between the water droplets and a solid impacting sample.

The specific objectives include:

1. Studying the water droplets impacting pattern on the surface with the use of ink coated samples.
2. Studying the airflow within the rotating disc rig and its effects on the water droplets using CFD simulation.
3. Investigating the water droplet interactions with multiple samples that have different surface geometries (flat, groove and porous structure) experimentally and by simulation.
4. Studying the formation of a water film and its effect on the WDE behavior.

Chapter 3: Experimental methodology

This chapter introduces the WDE experimental procedures and the parameter selections for the computational fluid dynamics (CFD) simulation of water droplet interactions with the impacting samples and the airflow turbulence during the WDE tests. The method used to measure the surface roughness of the test sample is presented in this chapter. The WDE test apparatus is also introduced. The data used for the CFD simulations is based on the experiments in this thesis. Ti-6Al-4V alloy was selected as one sample material in most of the tests performed in this thesis. A Nickel-Chromium (NC) foam was also employed as a secondary sample material to study the water droplet interactions with porous structure in this work.

3.1. Sample preparation

3.1.1. Ti-6Al-4V flat sample preparation

Ti-6Al-4V was the main alloy chosen in this study because it is a common alloy used in the compressor blades of gas turbines. All the flat reference samples are 23 mm (length) x 8 mm (width) x 3 mm (thickness) and shaped according to the drawing in Fig. 3-1 (a). Furthermore, for the WDE tests, the samples are affixed to the L-shape sample holders, as shown in Fig. 3-1 (b). Washers, screws, and nuts are employed to secure the sample in place to avoid it detaching from the holder during WDE tests.

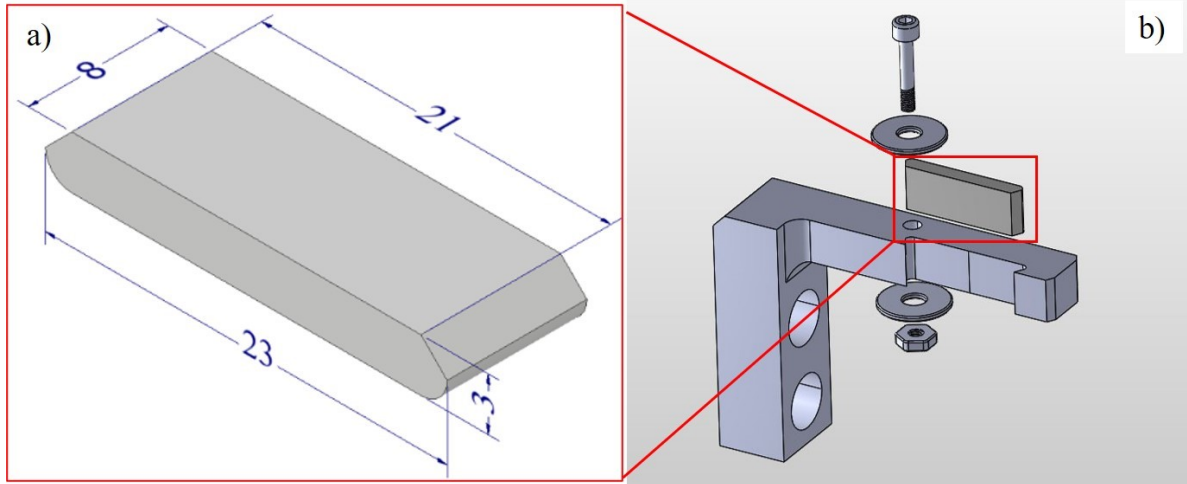


Figure 3-1 a) Ti-6Al-4V flat reference samples for low speed testing design b) Schematic of flat reference sample and sample holder assembling (Dimensions in mm).

3.1.2. Grooved sample preparation

Grooved samples have also been employed in this work. The width of the groove is determined and constrained to 4 mm based on the results from the water-flow pattern tracing experiment (discussed in section 3.2). Groove depths of 0.5 mm and 1 mm are machined at the center of two of the sample surfaces, as illustrated in Fig. 3-2 (a) and (b). The tests are performed for the grooved samples at 250 m/s. The bottom-blocked grooved samples are also employed to stabilize the water film further, as can be seen in Fig. 3-2 (c). All tested samples are weighed on an electrical balance (Ohaus, USA, accuracy: ± 0.2 mg). The pictures used to observe the behaviors of WDE before and after each erosion test cycle were captured with an optical microscope.

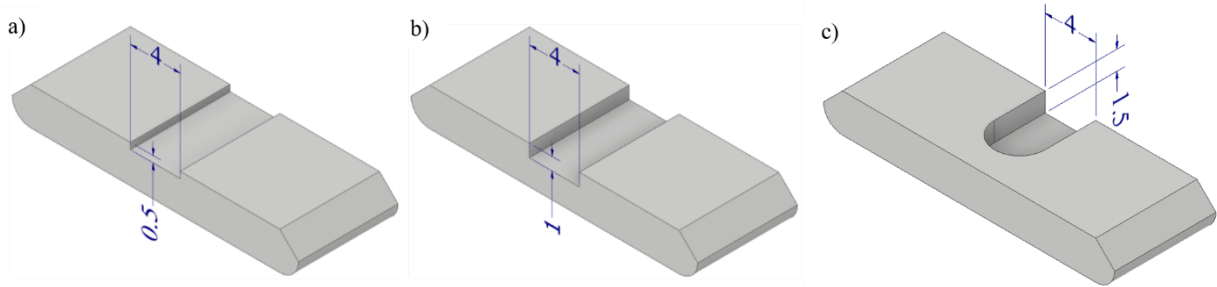


Figure 3-2 a) 0.5 mm depth grooved sample b) 1 mm depth grooved sample c) Bottom-blocked grooved sample (Dimensions in mm).

3.1.3. Metallic foam sample preparation

In order to stabilize the water film and study the effect of a porous structure to dampen the droplet impacts, the metallic foam samples are designed based on those with a groove. A Nickel-Chromium (NC) foam has been employed and affixed in the groove of the sample in this experiment. The metallic foam samples are provided by Recemat Pvt. Ltd, the Netherlands. The foam which is used in this work is shown in Fig. 3-3 (a). The technological properties of this metallic foam are presented in Table 3-1. The foam was cut by a low speed saw (Buehler, USA) and sized 8 mm length, 4 mm width and 1.7 mm thick, as shown in Fig. 3-3 (b). It was affixed in a 1.7 mm depth groove sample. Polyurethane was used to seal the pores of one of the foam samples to create a reference sample. This made the porous foam sample behave as a solid in the WDE test in order to emphasize the effect of the pores in damping the water droplet impacts.

Due to its highly elastic and durable nature, polyurethane has been used as the main protective coating on wind turbine blades to protect them from foreign body impact [56, 57]. Therefore, polyurethane coating has been employed to seal the pores in the metallic foam samples used for the WDE tests. In this work, the blocked metallic foams are used as reference samples. The purpose of using this reference sample is to create a valid comparison between

similar samples and to reveal the effect of the continuous porous structure in damping the droplet impacts. The tests were performed at 150 m/s for up to 20 minutes.

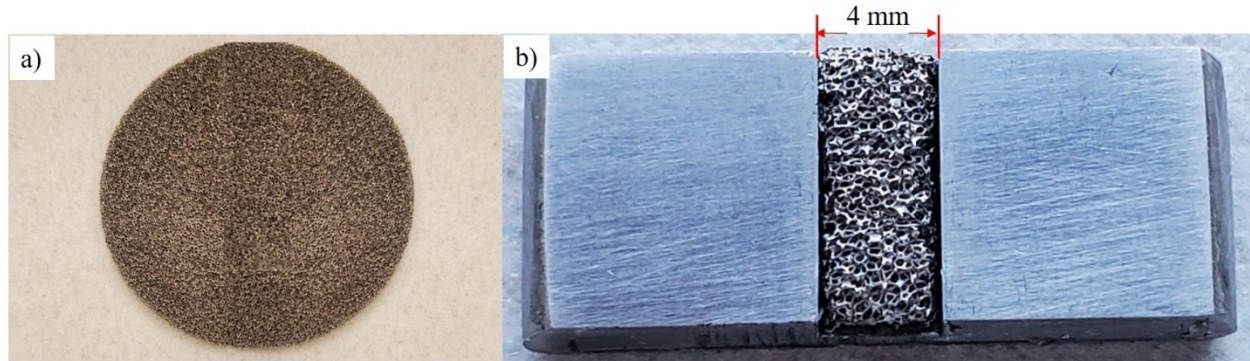


Figure 3-3 a) Nickel-Chromium metallic foam b) 1.7 mm depth grooved sample with metal foam filled.

Table 3-1 Properties of Recemat metallic foam

Pore size (mm)	Porosity (ϵ)	Density (Solid) (g/cm^3)	Density (Foam) (g/cm^3)	Estimated Specific Surface Area (m^2/m^3)	Surface Roughness [S_a] (μm)
0.4	0.84	5.16 ± 0.2	0.81	5400	109.53

3.1.4. Surface roughness

600 grit grinding paper was used to polish all samples in order to eliminate the effect of roughness on WDE behavior and to ensure that all samples have comparable levels of surface finish. In this thesis, surface roughness has been a constant parameter. A confocal laser microscope (Olympus, Japan) was used to inspect the surface roughness before performing every WDE test. S_a (the arithmetic average of area surface roughness), which is a common surface roughness parameter is used to determine the surface roughness of the reference and tested samples. The surface roughness results were measured 5 times (values S_a) and averaged. The averaged value is applied as the final surface roughness result in this thesis.

3.2. Water flow pattern tracing experiment

As mentioned previously, understanding the water droplet interactions with the solid sample are paramount for studying WDE behavior. First, the interactions are studied with the use of ink coated samples experimentally. The surface of the samples is coated with ink, as shown in Fig. 3-4. A permanent marker provides a unified and smooth layer of ink coating. Furthermore, as an oil-based ink, it does not flake off by the subsequent droplet impingement or peel off the base material. The ink pattern is recorded before and after the WDE test in order to detect the water droplet interactions with the solid sample. The experiment is conducted for a duration of 2 seconds; it is the minimum time that can be achieved. This is simply done by opening and closing the water droplet generator after attaining the required test speed. The reason to keep the duration time short is to avoid the droplet impingements from washing away too much ink. This minimizes the numbers of water impingements and reveals how water flowing and splashing during the test.

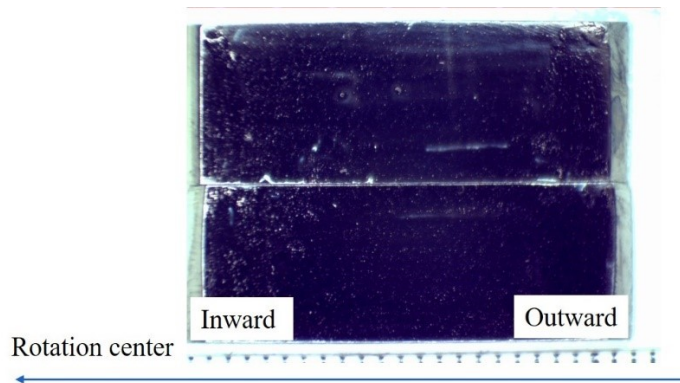


Figure 3-4 Oil-based ink coated samples.

Alcohol is used to clean the substrate before painting the ink layer and remove any remaining ink layer after the WDE tests. Compressed air is applied before painting to ensure no impurities remain and affect the water flow pattern during the WDE tests. Air is also used to dry the painted layer out. Three different testing speeds of 150 m/s, 200 m/s and 250 m/s are used in

this experiment in order to investigate the influence at each testing speed on the water flow pattern. The purpose of using the lower speeds is to observe more droplets impacting details from the ink coated sample after the impingements. Because a higher impacting speed causes more water droplet impingements in the same exposure time, thereby washing more ink away. The interactions between the water droplets and the solid impacting samples can be predicted approximately from the remaining ink pattern after the WDE tests.

3.3. Computational fluid dynamics (CFD) simulation

It is difficult to observe the actual experimental conditions where water droplets impact the samples during the WDE test. For this reason, simulating the same conditions present in the rotating disc rig using CFD is instrumental to study the interactions between the water droplets and the samples. This could help us better understand WDE behavior and improve ways to mitigate it. During the dynamic rotating tests, the water droplet interactions with the samples are mainly affected by the aerodynamic turbulence. Thus, in this work, the air turbulence and the interactions of the droplets with the impacting samples are both simulated. Ansys Fluent is employed to perform this CFD simulation. Most of the CFD parameters have been set according to the actual experimental data. The parameters of the test chamber conditions are shown in Table 3-2.

Table 3-2 Parameters of tested chamber conditions

Parameters	Chamber pressure (mbar)	Temperature (°C)
Experimental data	50	25

The key numerical parameters for the simulations in this work are presented in Table 3-3. The diameter of the computing domain is two times the rotation diameter of the sample, a cylindrical domain for the 3D simulation and a circular domain for the 2D simulation in this

work. The edge of the domain is defined as the outlet of the simulations. The droplets need to be patched in the simulations. It is worth mentioning that the porous media model is employed to simulate the case of porous metal foam in this work.

Table 3-3 Setups of the numerical parameters in the simulations

Phase flow model	Turbulence model	Mesh size	Boundary Condition	Wall function
Eulerian Multiple Fluid Modeling (Volume of fluid)	K-Epsilon	0.03 mm	Outlet: Pressure (0 Pa)	Scalable

3.4. WDE test and experimental apparatus

The WDE tests were conducted in a rotating disc erosion rig available at Concordia University, Montreal, Canada. The tests were conducted in accordance to ASTM G73-10 standard [28]. Fig. 3-5 (a) shows the experimental apparatus that simulates the high speed rotation of gas turbine blades for the WDE tests. This rig is mainly composed of a vacuum supplying system, a water droplet recycling system and a rotating disc. The droplet generator is connected to a water droplets generating system to release droplets when performing an erosion test cycle. A sample is placed on each side of the rotating disc during the WDE test, as shown in Fig. 3-5 (b). In order to keep the rig balanced and avoid vibrations, the mass summation difference of sample and sample holder on each side of the disc should not exceed 0.1 g. The droplets fall vertically creating a singular and precise water streak, impacting the sample rotating horizontally. The maximum linear speed of 500 m/s can be reached at the location where the water droplets impact the samples in the rig. The rig is operated under vacuum (50 mbar) to reduce the heat generated due to the friction between the disc and the air.

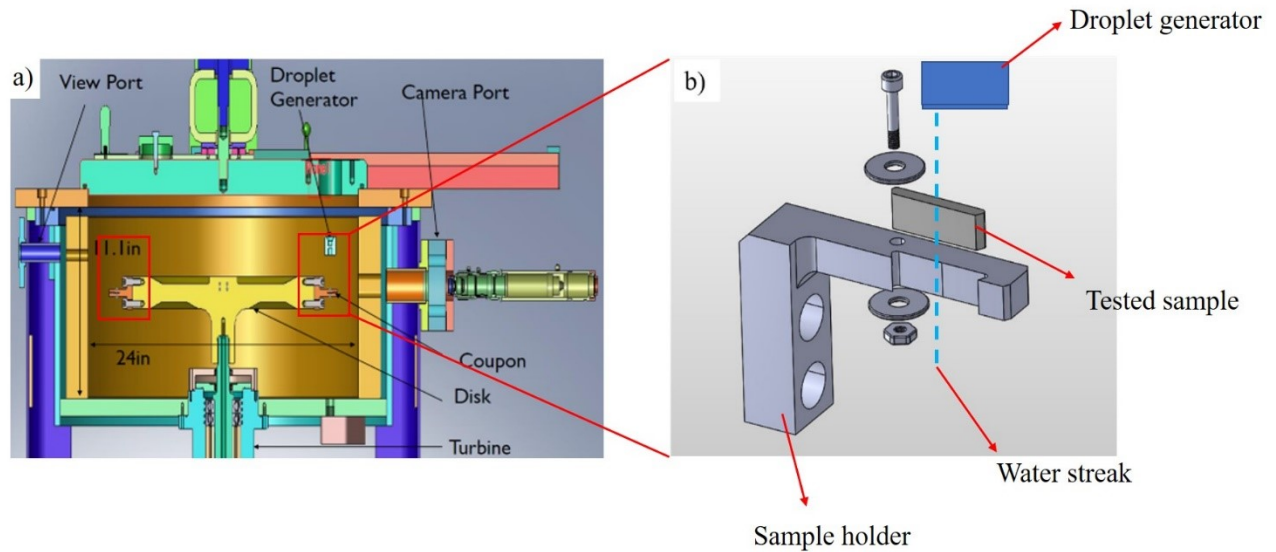


Figure 3-5 a) Schematic of the Water Erosion Rig b) Ti-6Al-4V flat reference samples for low speed testing design and sample holder assembly.

Several droplet nozzles are designed for this rig to generate different size droplets. Fig. 3-6 shows three different nozzles types: a) single-ray, b) three-ray and c) multiple-ray. In order to introduce the correct droplet size, the nozzle needs to be characterized before the tests, since several parameters influence the droplet size during the tests. In this work, the single streak nozzle is the only nozzle used in the WDE tests. Table 3-4 presents the conditions necessary to produce a 460 μm droplet size on average. The parameters are fixed during the WDE tests to ensure that all the results from the experiments in this work are comparable. Deionized water is used in this work to avoid clogging of the nozzles.

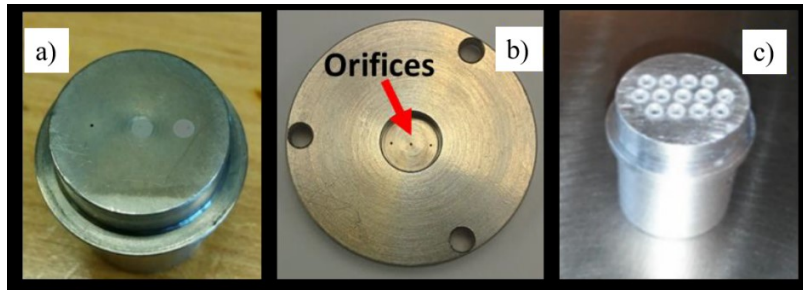


Figure 3-6 Nozzles used in the experiments (a) single-ray, (b) 3-ray, and (c) multi-ray (shower-head).

Table 3-4 Parameters for the single ray nozzle

Nozzle Name	Nozzle diameter (μm)	Water flow (liters/min)	Water line pressure (psi)	Number of Streak	Droplet size (μm)
Single-ray	400	0.05	1	1	460 ± 24.5

Chapter 4: Results and Discussion

4.1. Results of surface roughness measurements

The results of the samples surface roughness measured before the WDE test are presented in Table 4-1. The average values are listed in the last column. It can be observed that all samples have comparable surface roughness and approximate between 0.32 μm and 0.34 μm . Because the results are reasonably comparable, the surface roughness can be regarded to as a constant parameter in this work.

Table 4-1 Surface roughness of reference and tested samples

Surface condition	S_a [μm]					Average [μm]
Reference sample	0.317	0.375	0.349	0.338	0.330	0.342
0.5 mm groove	0.338	0.337	0.353	0.351	0.342	0.344
1 mm groove	0.311	0.332	0.323	0.323	0.312	0.320
Bottom blocked groove	0.330	0.325	0.343	0.314	0.338	0.330

4.2. Water flowing pattern tracing experiment

In order to study the water droplet interactions with the sample during the WDE tests, ink coated samples are employed to observe the imprints left by the water droplets. Fig. 4-1 shows the results of the water-flow pattern tracing experiments at 150 m/s, 200 m/s, and 250 m/s. The experiment is conducted for a duration of 2 seconds which is the minimum time that can be achieved before washing away too much ink. There are approximately 7 droplets colliding with the sample each rotation as reported by Kirols [58]. The number of water droplet impingements are calculated using equation (7):

$$N_{impingement} = n_{spr} \times t \times rpm, \quad (7)$$

where n_{spr} is the number of droplets hitting the sample each complete rotation, rpm is the number of rotations per minute and t is the time of exposure in minutes. The number of initial impingements at 150 m/s, 200 m/s, and 250 m/s test speeds within 2 seconds are presented in Table 4-2. From the experimental observation, more ink is removed as speed increases. This is considered to be due to the increased number of water droplet impingements as speed increases. Within the same 2 second time period, the higher test velocity causes a greater number of impingements removing more ink coating as can be seen in Fig. 4-1.

Furthermore, observation of the experimental results in Fig. 4-1 shows the sample surface is basically divided into three regions (according to the pattern recorded on the ink); intensive secondary droplets impact area, lateral jetting area, and a low secondary droplets impact area. The intensive secondary droplets area can also be divided into two subsections, region A and region B. Region A suffers more secondary droplets than region B, as shown in Fig. 4-1. Studying the pattern of secondary droplets is significant to understand the initial water droplet interactions with the solid sample. Since this has been observed at three different speeds, the three regions are likely to occur inherently in the WDE tests. Identifying the regions is beneficial to understand the interactions between water droplets and the sample.

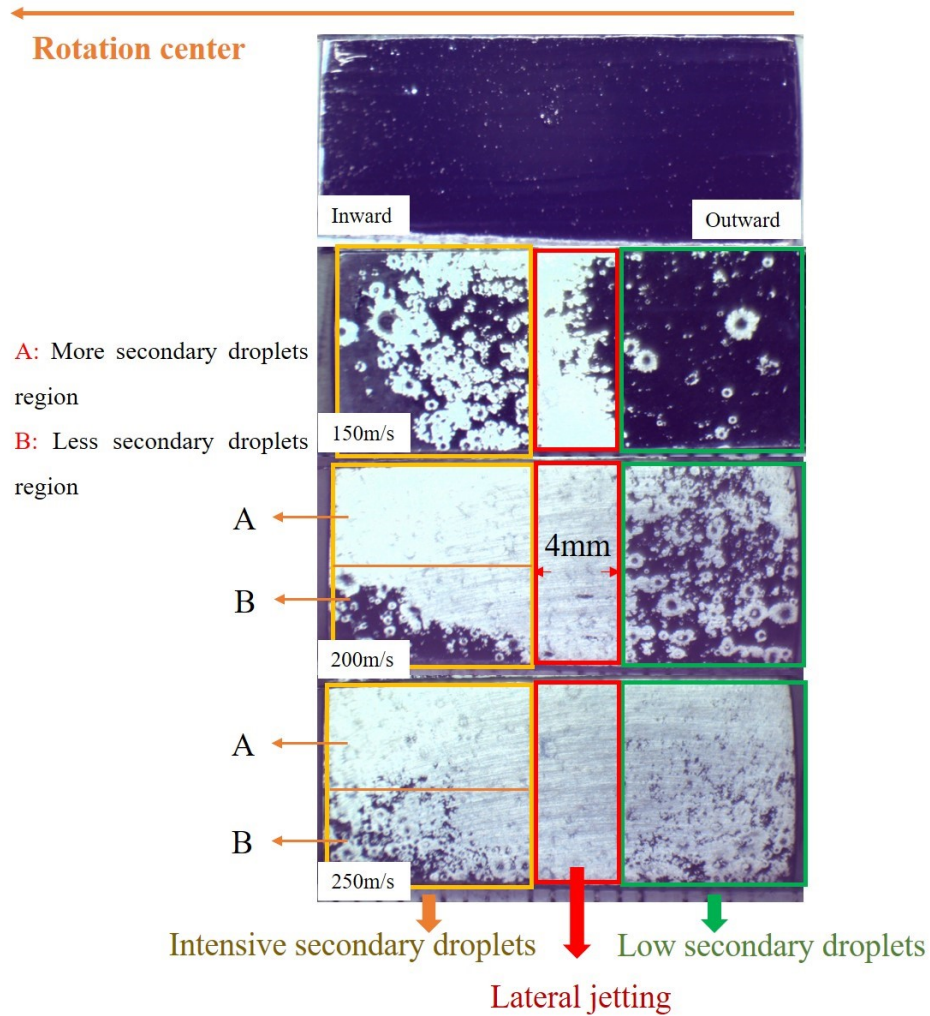


Figure 4-1 Ink coated samples after WDE test at 150 m/s, 200 m/s and 250 m/s.

Table 4-2 The number of impingements at 150 m/s, 200 m/s, and 250 m/s within 2 seconds

Impact speed (m/s)	150	200	250
Numbers of impingements	1338	1783	2229

Inspecting Fig. 4-1 shows more ink is observed on the low secondary droplets area (outward) than the intensive secondary droplets area (inward). This could be related to the radial velocity of the droplets. According to Moreira et al. [59], the splashing modes of a water droplet impacting a solid surface at 90 and 15 degrees are presented in Fig. 4-2 (b) and the impact angle

is defined in Fig. 4-2 (a). The droplet that impacts the solid at 15 degrees has a larger radial velocity than that at 90 degrees. According to Moreira's study, a larger radial velocity inhibits the formation of the crown splashing, especially on the side of the velocity direction [59], as can be seen in Fig. 4-2 (b) ($\alpha = 15^\circ$). This corresponds with the experimental observation in Fig. 4-1. During the WDE tests, the droplets encounter a radial velocity caused by the radial airflow.

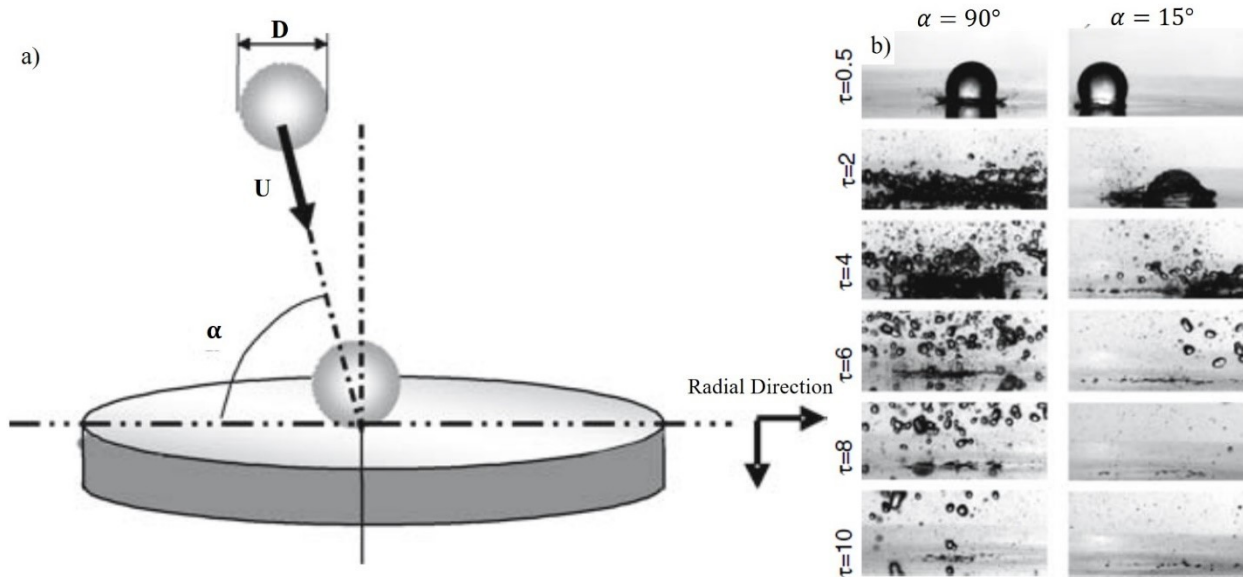


Figure 4-2 a) Definition of the impact angle α , D and U are, respectively, the initial diameter and the impact velocity of the primary droplet b) Effect of impact angle ($D = 2.75$ mm) $\alpha = 90^\circ$ $U = 2.5$ m/s and $\alpha = 15^\circ$ (τ : Time(s)) [59].

It is worth noting that the influence of the axial airflow is considered the main reason affecting the trajectories of the secondary droplets, thereby resulting in more secondary droplets impacting region A than region B. Investigating the airflow and its effects on the droplets during testing is significant to help understand the interactions between the water droplets and the impacting solid sample. The next section presents the simulation results of airflow and its effects on the initial and secondary droplets.

4.3. Influence of the airflow on the water droplets using CFD simulation

In this section, the effects of the airflow are discussed in three directions: The axial direction, the tangential direction and the radial direction. In order to avoid any confusion, Fig. 4-3 shows the directions of those three airflows throughout this chapter.

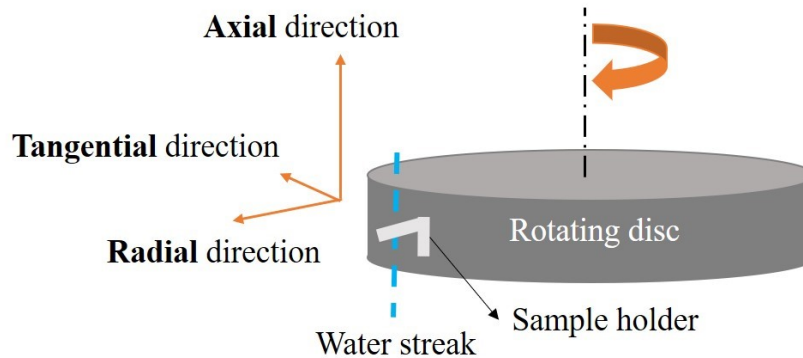


Figure 4-3 Airflow direction description figure.

4.3.1 Effect of the radial airflow

In order to understand the influence of the airflow on the trajectories of water droplets in this work, a simulation of airflow in the test chamber is carried out to help explain the experimental observations in Fig. 4-1. The outward radial airflow is reported by Herring et al. [44] and Sor et al. [45] in the form of sample wakes. Similar effects are presented in Fig. 4-4 (a) and (b). The sample causes air rotations in its wakes, as can be seen in Fig. 4-4 (a). The rotations and wakes produce a significant radial aerodynamic force. The wakes caused by the first sample hitting the droplet streak influence the water droplet streak hitting the subsequent sample during the rotation. At the same chamber position, the strength of the wakes reduces with the sample rotating away, as can be seen in Fig. 4-5. The light blue section represents the attenuated airflow produced by the sample ahead. When it approaches the subsequent sample, it begins to grow a stronger radial airflow again, as seen in Fig. 4-5. This stronger radial airflow provides a radial velocity to the impacting droplets in an outward direction. According to Moreira et al. [59], this

inhibits the formation of secondary droplets on the outward side which results in less secondary droplets on the sample right (outward) side, as shown in Fig. 4-1.

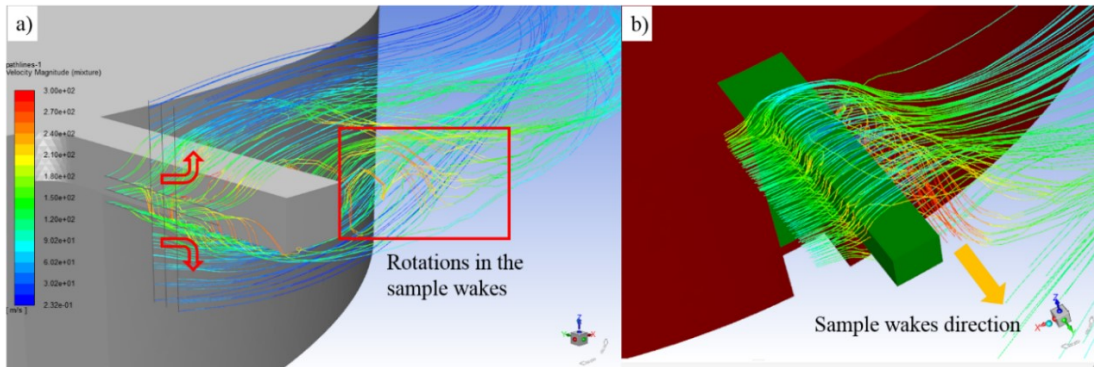


Figure 4-4 a) The airflow around the rotating sample and b) sample wakes at 250 m/s.

The red dash line in Fig. 4-5 basically demonstrates the mainstream trace of the airflow. Fig. 4-4 considers a steady airflow in front of the samples without the radial flow. However, Fig. 4-5 presents the presence of the radial flow in 2D in the test chamber during the WDE test at 250 m/s.

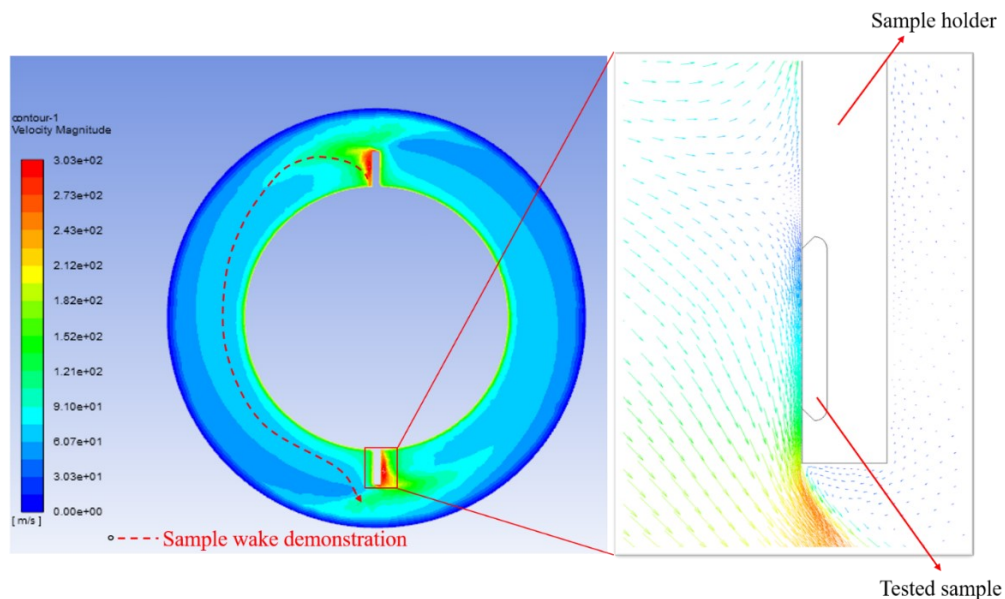


Figure 4-5 Samples rotating in clockwise direction at 250 m/s in the test chamber showing the distribution and the magnitude of the radial sample wakes.

According to the work of Hao et al. [60], one hypothesis for the splashing pattern with a radial velocity droplet was proposed. When the droplet obtains a radial velocity from the radial airflow, the gas surrounding the droplet moves at the same velocity as the droplet. When the droplet hits the substrate, the droplet forms a lamella that spreads along the substrate. Meanwhile, the surrounding gas keeps moving. When the gas encounters the spreading tip of the droplet, and the velocity direction of the gas is against the droplet's spreading direction, the spreading tip of the droplet is detached from the substrate by the gas. In the case where the velocity direction of the surrounding gas and the droplet's spreading direction are the same, the spreading tip of the droplet would not lift up. The process is sketched in Fig. 4-6. In the case of this work, the radial airflow contributes either to enhancing the splashing as in Fig. 4-6 (a) or to reducing the splashing as in Fig. 4-6 (b).

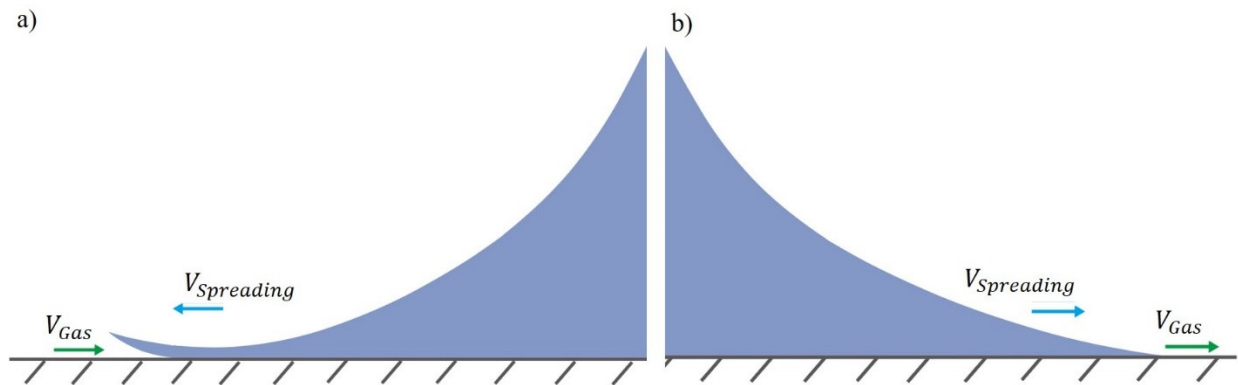


Figure 4-6 Sketch of a lamella a) The velocity directions of the gas and spreading are opposite b) The velocity directions of the gas and spreading are the same.

4.3.2. Effect of the axial airflow

This section will present the influence noticed in Fig. 4-4 of the airflow dividing into two parts axially in front of the sample. Fig. 4-7 (a) and (b) present the airflow passing the sample surface when the WDE tests are performed at an impact speed of 250 m/s. During the WDE tests,

the steady airflow in front of the sample is divided axially into upward and downward airflows. This can be seen in Fig. 4-7 (a) and the dividing line is presented in Fig. 4-7 (b). The two diverging airflows are opposite in direction and therefore have different effects on the falling water droplets before hitting the sample. When the rotating sample approaches the falling droplets, the downward airflow surrounding the sample accelerates the droplets falling down. On the contrary, the upward airflow produces resistance (deceleration) to the water droplets. This effect results in more droplets impacting the upper portion of the sample while fewer droplets impacting the lower portion. This may cause the top of the sample to erode faster than the bottom half. This can explain the WDE damage appearance reported in [61, 62].

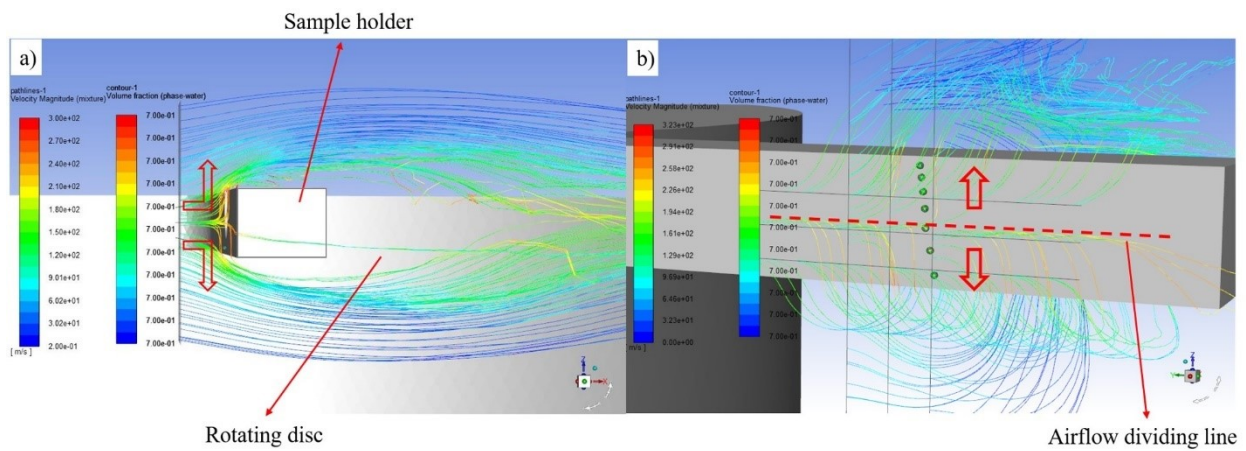


Figure 4-7 a) Side view of the simulated airflow graph b) Airflow with dividing line.

Due to the secondary droplets having less mass, they can be easily influenced by the airflow. Here, the airflow decelerates the secondary droplets above the dividing line and accelerates the secondary droplets below the line. This results in fewer secondary droplets impacts in region B as seen in Fig. 4-1. Furthermore, due to the airflow accelerating the droplets below the dividing line, the initial and secondary droplets have a larger downward velocity that results in less splashing on the downward side. This corresponds with the explanation in the

work of Moreira et al. [59] and Hao et al. [60]. For this reason, one could argue that fewer impingements and less splashing of secondary droplets in region B are the two main reasons for the observed ink pattern on the inward side area in Fig. 4-1.

4.3.3. Effect of the airflow on the impact angle

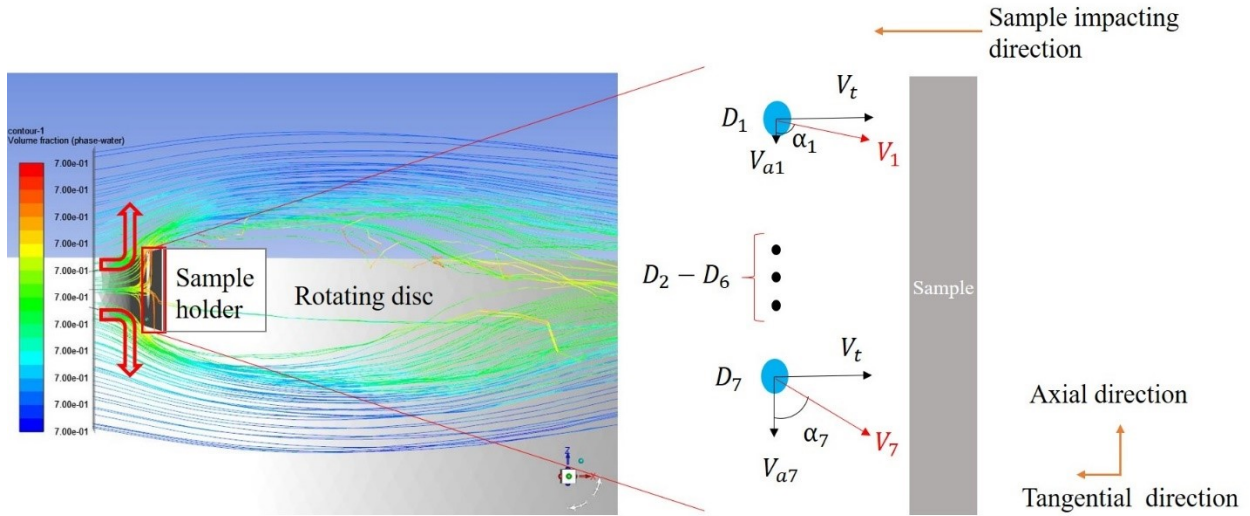


Figure 4-8 Schematic for the impact angles influenced by the airflow.

Fig. 4-8 presents the impact angle which is influenced by the axial airflow. D_1 - D_7 represents the falling droplets from the first to the last in the impacting section of the water streak. D_1 and D_7 are the typical droplets in the upper and the lower portion of the impacting section of the water streak, respectively. Thus, these two droplets are analyzed in this work. V_{a1} and V_{a7} are the axial speed of the first and last droplets in the impacting section of the water streak. Since the droplets are affected by the axial airflow as mentioned early, V_{a7} is larger than V_{a1} . Moreover, V_t is the relative speed between droplets and the sample in tangential direction and equal to the value of impacting velocity (250 m/s). Thus, angle α_1 is larger than angle α_7 , which means the upper droplets have an impact angle closer to 90 degrees than the lower droplets. However, the difference between angle α_1 and α_7 is found to be less than 2 degrees for

the current work. Hence, the difference in impact angle from D_1 - D_7 is insignificant and can safely be neglected [38] in this work.

Fig. 4-9 presents the simulation results of water droplets impacting the sample at 250 m/s. The water droplet streak is shifted by the radial airflow, as mentioned in Fig. 4-5 and presented in Fig. 4-9. The simulation results of lateral jetting correspond with the experimental results in Fig. 4-1. The maximum width of the lateral jetting is slightly less than 4 mm both experimentally and by simulation. Since the lateral jetting lamella could play a potential role in creating a water film that dampens the energy of an impacting droplet, hence reducing WDE damage, the jetting lamella is studied in the next section.

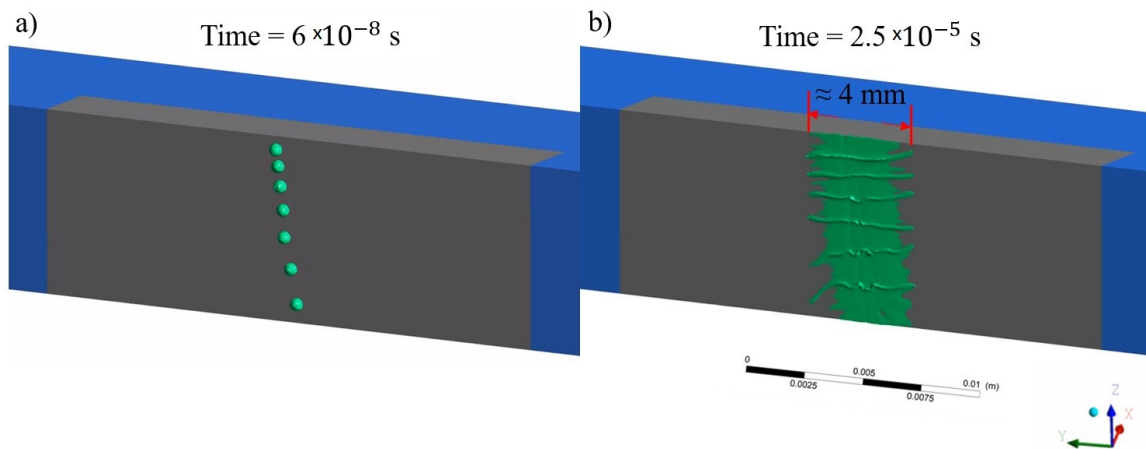


Figure 4-9 Simulation results of droplets impacts on the rotating sample at 250 m/s a) Initial moment b) Estimated maximum width distance of lateral jetting from the simulation.

4.4. Understanding the water droplet interactions with 4 mm width grooved samples

4.4.1. WDE tests

In order to better understand the influence of how the water droplets interact with a solid impacting sample and study the effect of a water film, a sample is machined with a 4 mm width groove (equal to the estimated maximum lateral jetting distance) on its surface. There are a few reasons for machining a 4 mm width groove:

1. Based on the results of the ink experiment in Fig. 4-1 and the simulation in Fig. 4-9, the lateral jetting distance is approximately 4 mm.
2. If the groove is too narrow, the lateral jetting may cause hydraulic penetration.
3. The drift distance of the water droplets streak is determined experimentally to be around 1 mm. Despite the drift in the water droplets streak, the impacts should be contained within the groove.
4. If the width is more than 4 mm, there will be not much difference between the flat sample and the grooved samples.

Two different depths of 0.5 mm and 1 mm were selected for the grooved samples tests that will be compared with the flat sample. Fig. 4-10 shows the relationship of mass loss vs. time exposure for 2 grooved samples and the flat reference. The incubation period and maximum erosion rate are extracted from the intersection of the line drawn along the x-axis and slope of the line, respectively. During the test, the flat sample started to erode first near the 40-minute mark, as shown in Fig. 4-10 and Table 4-3. The samples with grooves experienced a longer incubation period than the flat one. Comparing the grooved samples, the 0.5 mm groove has a slightly better WDE performance than 1 mm groove. For instance, after 60 minutes of WDE testing, the reference sample encountered a 0.0045 g mass loss as shown in Fig. 4-10, Fig. 4-11, and Table 4-3. The 1 mm depth grooved sample began to exhibit some erosion, but the 0.5 mm depth grooved sample had yet to display any erosion. These results are summarized in Table 4-3. However, when the maximum erosion rate stage is reached, there is barely any noticeable difference between the flat reference and grooved samples (0.5 and 1 mm) as they all display the same erosion rate. One plausible explanation for the observed longer incubation period of the grooved samples is the formation of a protective water film during testing. According to

Honegger [27] and Heymann [25], the water film serves as a cushion that dampens the impact energy from subsequent droplet impacts. When erosion craters develop, the water film effect is diminished and other erosion mechanisms, such as hydraulic penetration, dominate the subsequent stages.

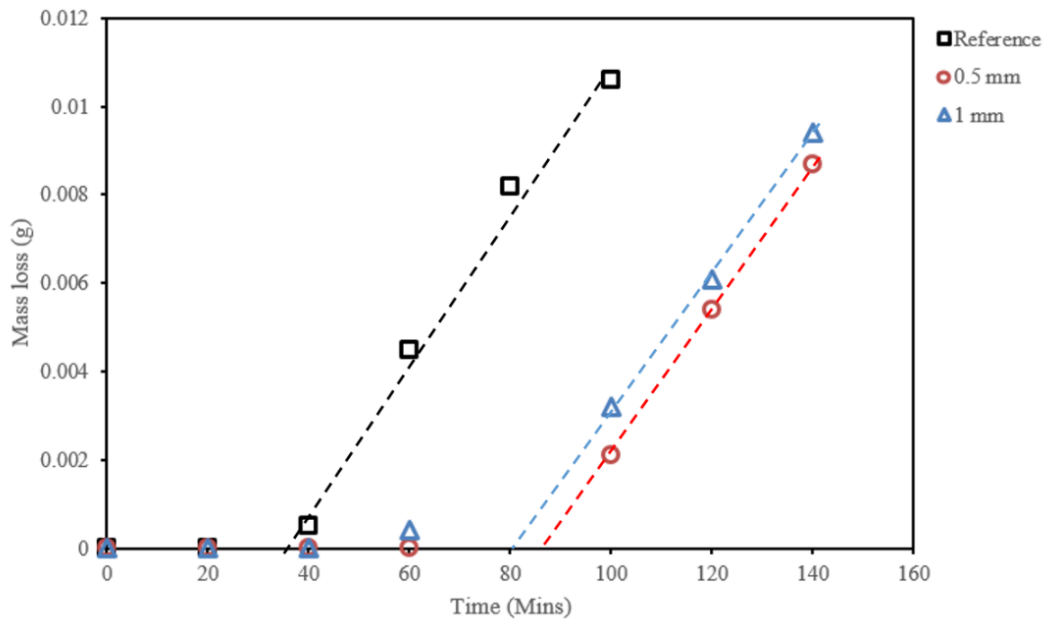


Figure 4-10 Erosion curve with different depth grooves.

The optical macrographs of samples from the WDE tests are shown in Fig. 4-11. This figure shows that the grooved samples have an incubation period approximately two times longer than the flat reference sample. Most of the erosion starts at the top of the sample because the top section has more intensive impact droplets compared with the bottom section. These experimental results correspond with the influence of the airflow decelerating the droplets above the airflow dividing line as discussed earlier.

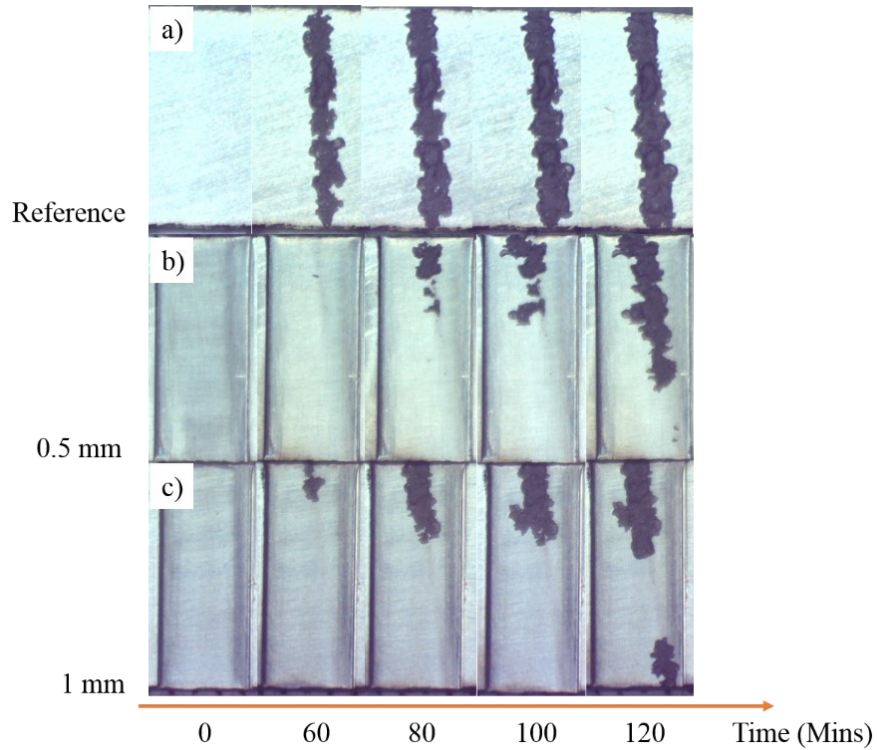


Figure 4-11 WDE test results a) reference sample (0 mm) b) 0.5 mm groove sample c) 1 mm groove.

Table 4-3 The mass loss of reference, 0.5 mm depth groove, and 1 mm depth groove sample in the first 60 minutes of testing.

Time (Mins)	Mass loss (g)		
	Reference	0.5 mm	1 mm
0	0	0	0
20	0	0	0
40	0.0005	0	0
60	0.0045	0	0.0004

4.4.2. Simulation of water droplet interactions with the grooved samples

In order to understand the effect of the water film during the WDE tests, the time of the impact for one full rotation (T) needs to be calculated with equation (8):

$$T_{full\ rotation} = \frac{\pi D_{disc}}{v}, \quad (8)$$

where D_{disc} is two times of the distance between the impact location and the center of the disc and v is the impact speed of the water droplets. The time of one full rotation for the disc with a diameter of 0.5 m at an impact velocity of 250 m/s is 6.28×10^{-3} seconds. Fig. 4-12 (a), (b), and (c) present the simulation of a water film created by the flat sample, 0.5 mm depth grooved sample, and 1 mm groove depth sample at 250 m/s, respectively. After around 6.3×10^{-3} seconds, the water disappears gradually on the surface of the flat sample. As for the 0.5 mm and 1 mm depth grooves, some of the water film is still remaining in those grooves as seen in Fig. 4-12 (b) and (c).

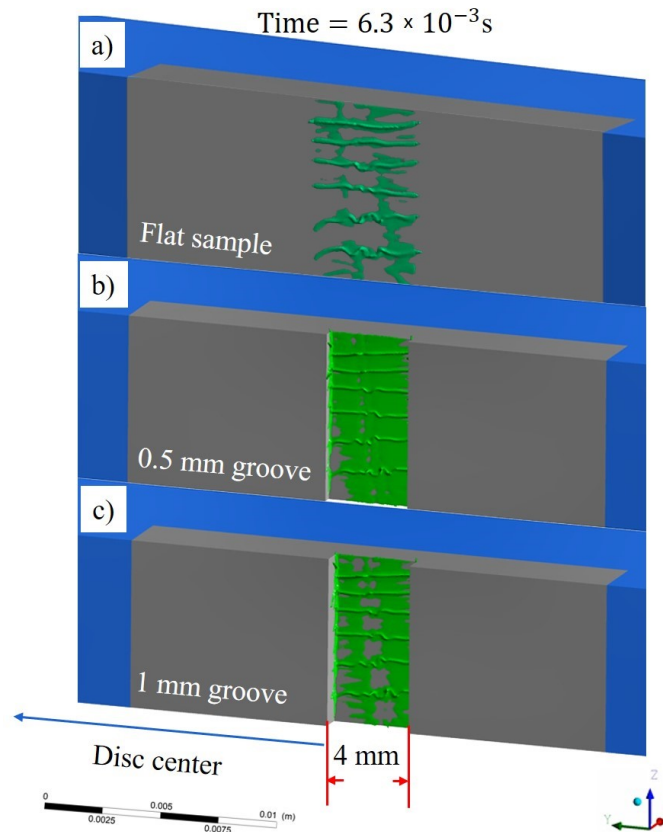


Figure 4-12 Water flowing mode simulation on a) flat sample b) 0.5 mm depth grooved sample c) 1 mm depth grooved samples at 250 m/s after one full rotation and prior to the next impact.

However, the airflow in both grooves behaves differently. This is considered the main reason that slightly influences the length of the incubation time of both grooved samples. The airflow patterns in both grooves are presented in Fig. 4-13 (a) and (b). The samples are rotating clockwise. It is clear that the magnitude of the airflow speed inside the groove is much lower than outside the groove. Thus, the water in the groove is believed to linger longer than the water on the surface of the flat sample. In addition, one can see from Fig. 4-13 (a) that in the bottom section of the 0.5 mm groove, the air has the same flowing direction as the lateral jetting. This appears to stabilize the water film. While in the left bottom section (outward) of the 1 mm groove, the air flows in the opposite direction of the lateral jetting direction, seen in Fig. 4-13 (b). The opposite airflow in the 1 mm groove appears to agitate the water film. This results in an unstable water film in that 1mm depth groove. In order to try a different approach to stabilize the water film further, a bottom-blocked sample is employed in this work and presented in the next section.

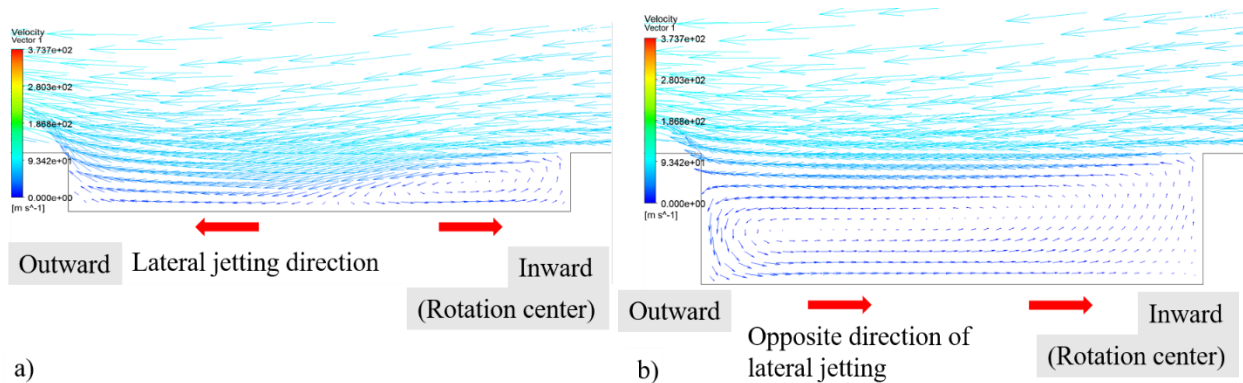


Figure 4-13 Air turbulence simulation in a) 0.5 and b) 1 mm depth grooves.

4.4.3. WDE tests with the bottom-blocked groove sample

A bottom-blocked groove, shown in Fig. 4-14 (a), is machined on the surface of the sample. The droplets are also divided by the dividing line as shown in Fig. 4-14 (b). As

mentioned earlier, the upper and lower droplets are also decelerated and accelerated respectively when the sample approaches the water streak. Interestingly, for the bottom-blocked grooved sample, the erosion begins at the bottom corner of the groove after 40 minutes as shown in Fig. 4-14 (a).

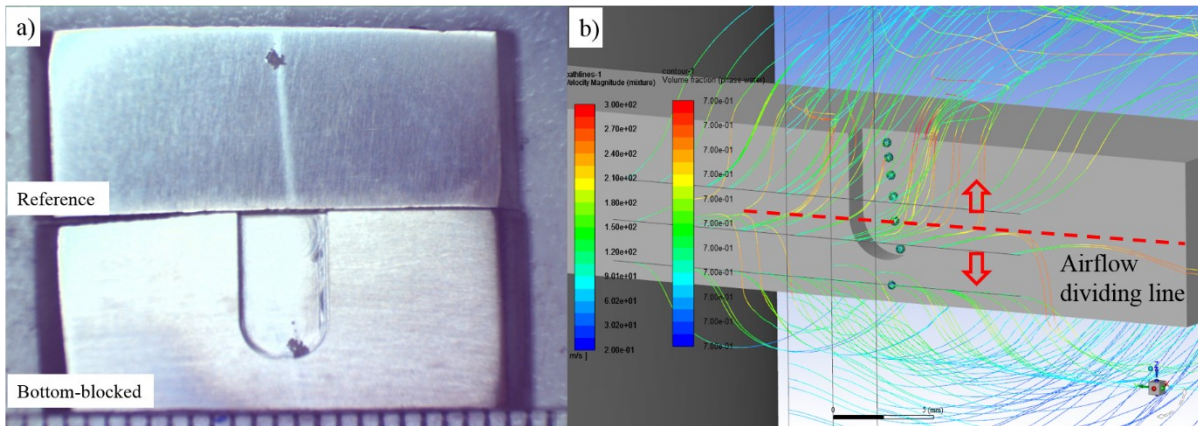


Figure 4-14 a) WDE test with bottom-blocked sample at 250 m/s after 40 mins. b) Simulated airflow graph of the bottom-blocked sample.

There are three plausible reasons that may have caused the erosion damage to begin earlier:

1. The interactions between the impacting water droplets with the bottom-blocked sample is simulated and shown in Fig. 4-15 (a) and (b). The droplet which impacts closest to the bottom of the groove is of concern. When this droplet impacts the sample, the jetting happens radially. A simplified description of the jetting can be defined as “horizontal jetting” and “vertical jetting”. These are presented with arrows in Fig. 4-15 (a). In the case of the droplet closest to the bottom of the groove, the “vertical jetting” strikes the bottom first. Then, it continues spreading along with the shape of the groove until it merges with the horizontal jetting. After repeated impingements at 250 m/s, the bottom corner of the groove may encounter damage earlier due to the multiple “vertical jetting”

strikes.

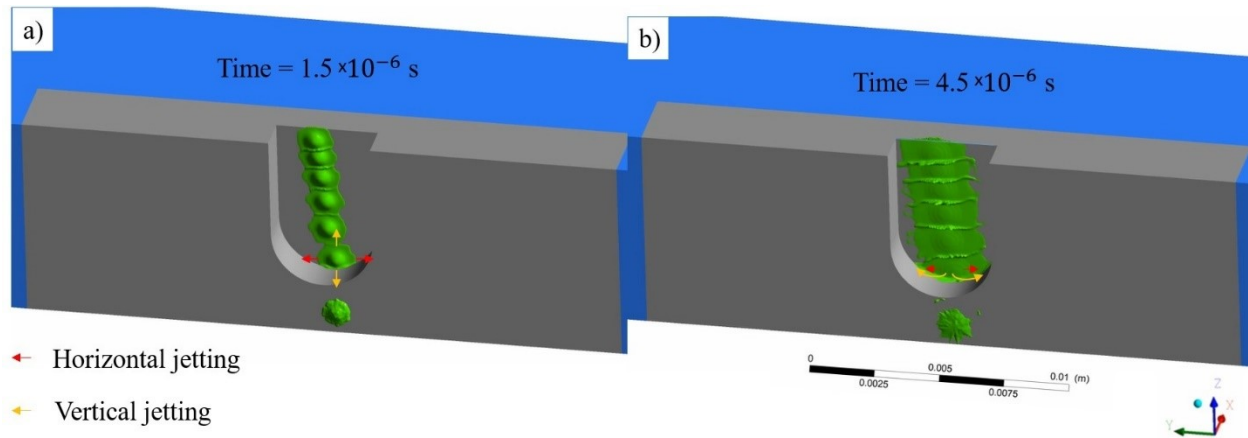


Figure 4-15 Simulation of the interactions between the impact droplets and the bottom-blocked sample a) after 1.5×10^{-6} s b) after 4.5×10^{-6} s.

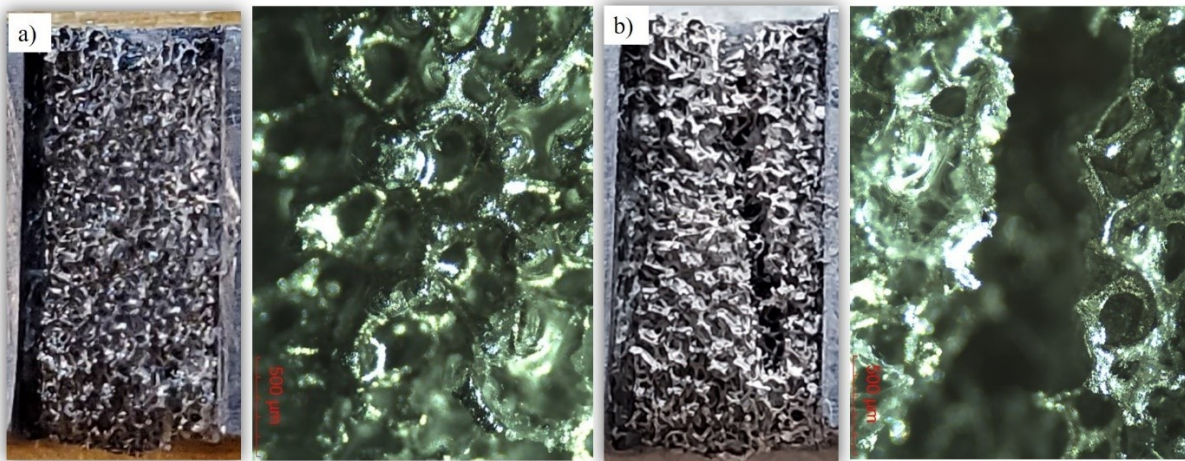
2. The airflow in front of the sample accelerates the downward droplets and makes these droplets obtain a higher impact speed at the corner of the groove compared to the rest of the groove.
3. Hydraulic penetration may cause faster damage during the continuous impingement due to the presence of an edge at the bottom of the groove.
4. The stress concentration at the bottom edge is also one of the reasons that likely cause erosion damage to begin earlier.

Since the bottom-blocked samples are not very effective at mitigating the damage from WDE compared to the flat reference samples, metal foam filled groove samples are employed to provide a damping medium for the impacting droplets in order to stabilize the water film and further study the water droplet interactions with the porous in relation to the solid samples.

4.5. Understanding the water droplet interactions with the metallic foam filled groove sample

4.5.1. WDE tests

The experimental results for the metallic foam, with and without polyurethane, are presented in Fig. 4-16. The samples are photographed with the use of an optical microscope. It can be observed from Fig. 4-16 (a) and (b) that while only slight damage can be seen on the foam sample, the polyurethane-blocked foam suffered significant damage from the water droplets. The polyurethane-blocked metallic foam followed the same WDE behavior as the solid material samples; an erosion line formed in the position where the water droplets impact. On the contrary, the porous metallic foam without polyurethane shows little erosion in Fig. 4-16 (c) and (d). The damaged regions of the metallic foam are highlighted by the red circles (Fig. 4-16 (d)). Only a few connections of the foam are broken after 20 minutes of WDE testing.



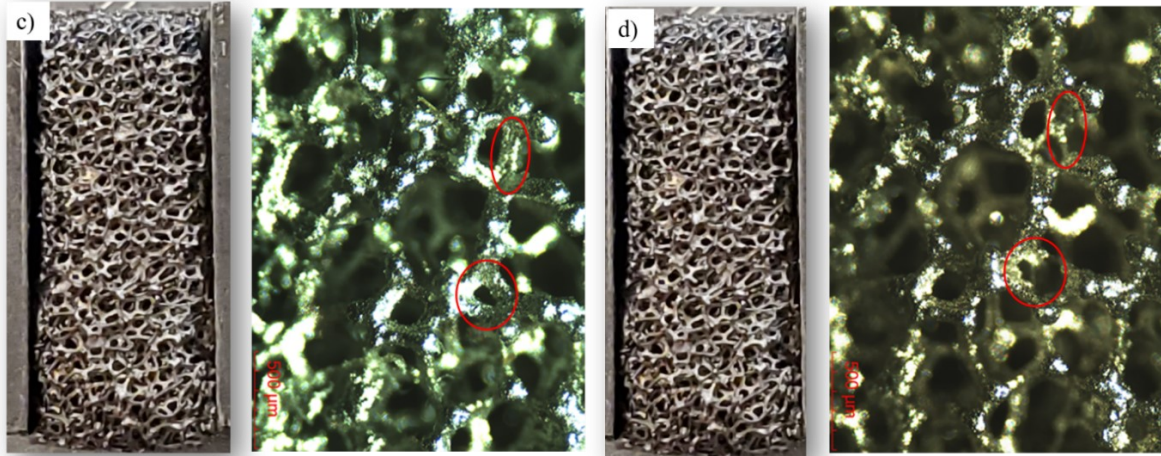


Figure 4-16 a) Initial metallic foam with polyurethane-blocked b) Metallic foam with Polyurethane-blocked, after 20 mins WDE test at 150 m/s c) initial metallic foam d) metallic foam after 20 mins WDE test at 150 m/s.

4.5.2. Simulation of impacting pressure on the metallic foam

Impact pressure is simulated to help understand the effect of porous structures on the WDE behavior. In order to build up porous metallic foam model in Ansys Fluent, Forchheimer's model [63], which is the most popular flow resistance model, is applied in this work. The equation used here is presented as follows:

$$\frac{\Delta p}{L} = au + bu^2, \quad (9)$$

where $\frac{\Delta p}{L}$ is the pressure gradient of the metallic foam, u is the flow velocity, a is the viscous resistance coefficient, and b is the inertial drag coefficient. The variables a and b are hydrodynamic characteristics linked to the structure of the metal foam, and they can be calculated from fluid pressure drop experiments. Air is the most commonly used fluid because its pressure drop is easier to measure [64]. In this work, a and b are calculated from the work of Mostafid [54]. The results are presented in Fig. 4-17. The different lines present different

thicknesses of foam. In this work, the solid line that presents the 1.7 mm thick metallic foam is the only line used to calculate the viscous resistance coefficient a , and inertial drag coefficient b . The remaining parameters for the simulation are based on the data provided by Recemat Pvt. Ltd in Table 3-1.

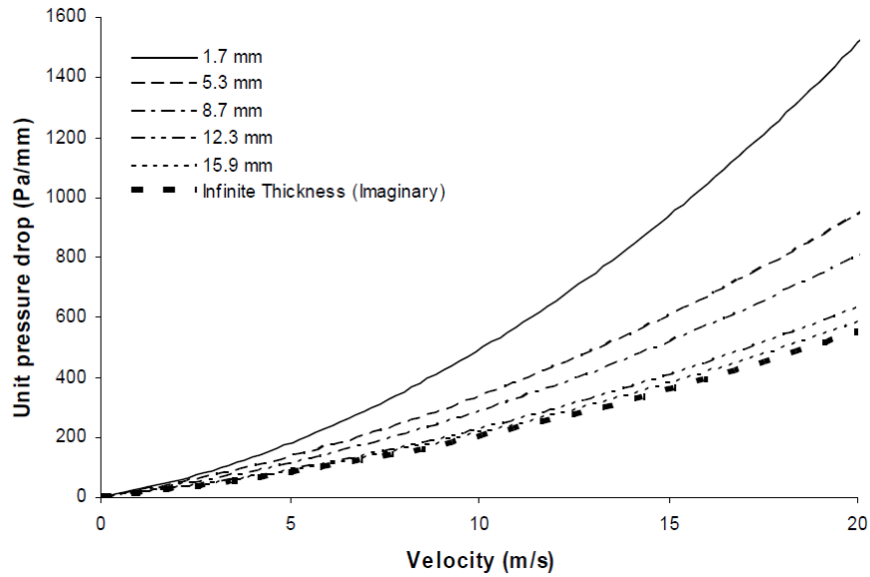


Figure 4-17 Pressure drop curve for NC4753 [54].

The porous media model and solid model are employed to simulate the structure of the porous metallic foam and polyurethane-blocked foam, respectively, using Ansys Fluent. The maximum pressure on the contact surface is monitored for the porous foam and polyurethane-blocked foams as shown in Fig. 4-18.

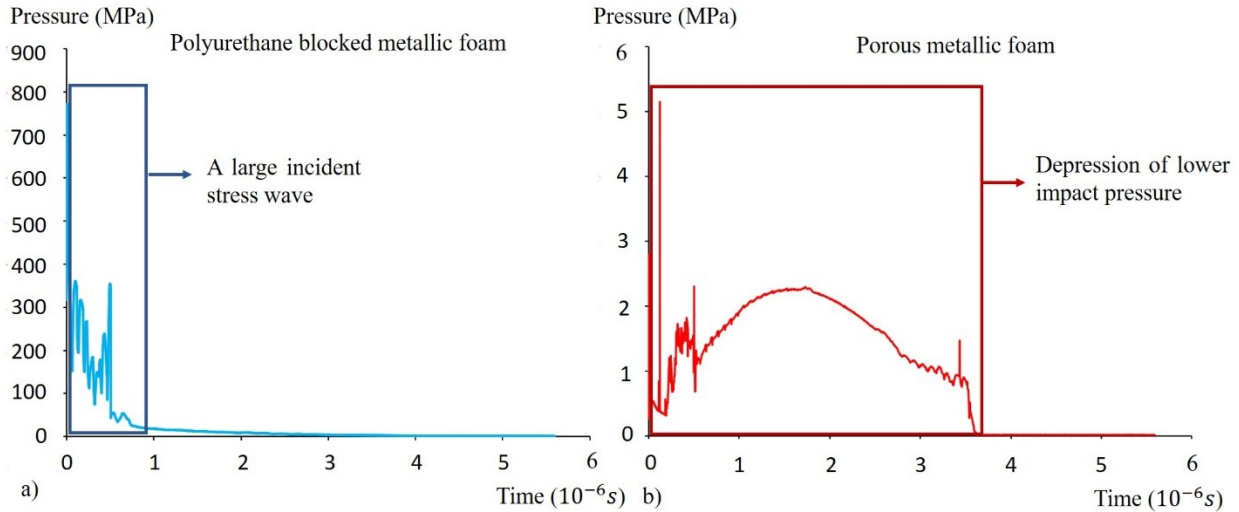


Figure 4-18 Pressure monitoring chart of contact surface for a) Polyurethane-blocked metallic foam b) porous metallic foam.

For the polyurethane-blocked foam, the value of peak pressure on the contact surface is around 780 MPa which occurs once the droplet reaches the surface, and the contact pressure reaches the peak and drops within a very short exposure time (Fig. 4-18 (a)). This represents a large pulse as an incident stress wave that causes severe damage. The pressure transmission process has been demonstrated in Fig. 4-19 (a). When comparing the peak value of the contact pressure on the porous metallic foam sample of about 5.2 MPa and peak pressure on the polyurethane-blocked metallic foam, one can clearly see that it is more than a hundred times that of the porous metallic foam sample. Thus, despite the maximum pressure lasting such a short time period, the polyurethane-blocked sample suffered large amounts of damage after repetitive impingements. This could explain why the solid polyurethane-blocked foam shown in Fig. 4-16 experienced more aggressive damage compared to the porous metallic foam that showed minimal damage. This could be attributed to the small peak pressure, as can be seen in Fig. 4-18 (b).

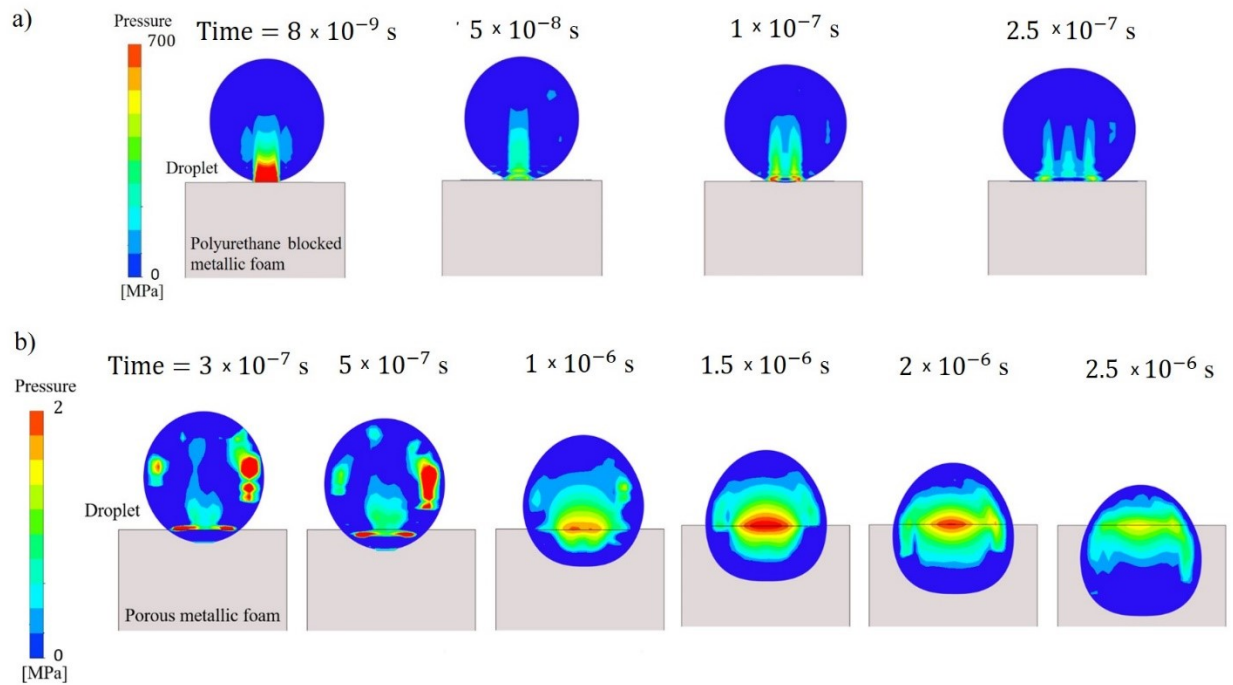


Figure 4-19 Time variation of pressure during the WDE test on a) polyurethane-blocked metallic foam b) porous metallic foam.

For the porous metallic foam, there are two pressure peaks appearing during the WDE process. The pressure transmission process for the porous metallic foam is demonstrated in Fig. 4-19 (b). The second pressure peak forms gradually after the first 5.2 MPa pressure peak, as can be seen in Fig. 4-18 (b). Then, the second peak, which is around 2.3 MPa, reduces slowly and uniformly. This represents the dissipation of lower impact pressure during a much longer duration (3.5 μ s) compared to the pressure dissipation in the polyurethane-blocked sample in Fig. 4-19 (a) (Time = 2.5×10^{-7} s). The damping of the impact pressure is obvious in the porous metallic foam sample.

Chapter 5: Conclusions, Contributions and Recommendations

The main conclusions of this work are summarized in this chapter. This chapter also highlights some contributions of this work and includes recommended suggestions for future work on this topic.

5.1. Conclusions

This work studied the airflow characteristics during the WDE tests and their effects on the water droplet interactions with various solid target materials by performing experiments and CFD simulations. Flat and grooved samples of different geometries were used to study the airflow and how that airflow affects the trajectories of droplets when impacting samples. In order to reveal different aspects of those interactions, samples with different surface features were used in this work including: flat, grooved, and metallic foam. The WDE tests were performed at 150 m/s, 200 m/s and 250 m/s for the ink coated samples, at 250 m/s for the grooved samples, and at 150 m/s for the porous and non-porous metallic foam-filled grooved samples. 250 m/s was also selected when performing the CFD simulation. An average droplet size of 460 μm was used in this thesis. From this work, it can be concluded that:

1. When the droplets have a fixed size of 460-micron meters, the lateral jetting has a maximum approximate distance of 4 mm at the three different speeds.
2. The falling droplets are not only influenced by the axial divided airflow but also by the radial airflow that is caused by the wakes of the previous rotating sample.
3. The radial airflow causes the water streak to drift radially outwards and creates a radial velocity to the impacting droplets. The radial velocity influences the formation rate of splashing. This causes more secondary droplets at the side closer to the rotation center than the farther side. The axial airflow influences the number of impacting droplets on the

different regions of the sample. The sample suffers more droplet impingements on the top half than the bottom half. Therefore, the top of the sample erodes faster than the bottom. The axial airflow also influences the impact angle to some extent. However, the impact angle is around 90 degrees and the change of it is insignificant; it can be safely neglected in this work.

4. A water film forms when artificial grooves present on the surface of the sample; this water film helps to absorb the energy of the droplet impacts. The water film increases the incubation period, but it does not influence the erosion rate once craters occur.

5. The 0.5 mm depth groove was better at mitigating WDE damage than the 1 mm groove. This is because the airflow characteristics are influenced by the depth of the groove. The 1 mm groove experienced a more complex airflow environment than that of the 0.5 mm groove and results in a less stable water film formation in the 1 mm groove.

6. WDE damage of the bottom-blocked groove sample starts at the innermost bottom corner of groove and the incubation period is similar in time to the flat reference samples.

7. A porous structure material was better at mitigating WDE damage than the solid material. This observation could also be explained by the CFD simulation. During the WDE test, the impact pressure of the water droplets was dissipated by the porous metallic foam; while the solid polyurethane-blocked foam encountered severe damage due to much higher impact pressure.

5.2. Contributions

This work investigates the airflow under vacuum (50 mbar) at a high speed (250 m/s) during WDE tests experimentally and by simulation, which is a first. The characteristic of the airflow and how they affect the water droplets are described in the present work. The WDE performance of the grooved and porous metallic foam filled samples are investigated by

experimentation and simulation. The effect of water film stabilization and WDE impact pressure dissipation are described and explained in this work.

5.3. Recommendations and future work

Since the present work considers many different parameters, a future work could change the value of certain parameter to study the effects of the airflow on the water droplets and the water droplet interactions with the solid impacting sample. Some recommendations for future work are:

1. Using droplets of different size could be a way to investigate the effects of the airflow on heavier or lighter water droplets.
2. The experiments performed in this work do not investigate how the porous metallic foam absorbs energy when the foam is filled with water instead of polyurethane. Therefore, there could be a simulation to investigate the damping effect of water filled foam. This can be achieved through the use of metal foams with different pore size.
3. Studying the influences of different pore sizes of the metallic foam on the peak value of the impact pressure is suggested. Perhaps an optimum size that leads to a stable water film and no WDE can be found.
4. The use of a high-speed camera is suggested to record the actual situation within the test chamber during the WDE test. This could help understand WDE further.

References

- [1] M. A. Ehyaei, A. Mozafari, M. H. Alibiglou: Exergy, economic & environmental (3E) analysis of inlet fogging for gas turbine, *Energy*, Vol. 36, No. 12, 2011, pp. 6851-6861.
- [2] M. Ameri, H. Nabati, A. Keshtgar: Gas Turbine Power Augmentation Using Fog Inlet Air-Cooling System, *Proceedings of the 7th Biennial Conference on Engineering Systems Design and Analysis 2004*, Manchester, England, Jan. 2004, pp. 73-78.
- [3] L. Maryam, B. Givi, X. Li: Performance Analysis of Fogging Cooled Gas Turbine with Regeneration and Reheat under Different Climatic Conditions. *Proceedings of the ASME 2014 Power Conference*, Baltimore, Maryland, USA, Jul. 2014, pp. 1-8.
- [4] T. Giampaolo: *The gas turbine handbook: Principles and practice*, 3rd edition. Fairmont Press, New York, USA, 2006.
- [5] J. R. Khan: PhD dissertation: Fog cooling, wet compression and droplet dynamics in gas turbine compressors. University of New Orleans, USA, 2009.
- [6] [Http://www.mdscoating.com/technology/index.html](http://www.mdscoating.com/technology/index.html), as on 28th Feb 2021.
- [7] A. K. Gujba, M. Medraj: Laser peening process and its impact on materials properties in comparison with shot peening and ultrasonic impact peening, *Materials*, Vol. 7, 2014, pp. 7925-7974.
- [8] M. Dina, A. Mostafa, D. Kevorkov, P. Jedrzejowski, M. Pugh, M. Medraj: Water Impingement Erosion of Deep-Rolled Ti64, *Metals*, Vol. 5, No. 3, 2015, pp. 1462-1486, doi: 10.3390/met5031462.

- [9] H. S. Kirols, D. Kevorkov, A. Uihlein, M. Medraj: Water droplet erosion of stainless steel steam turbine blades, *Material Research Express*, Vol. 4, 2017, pp. 1-12.
- [10] M. S. Mahdipoor: PhD dissertation: Water Droplet Erosion Resistant Materials and Surface Treatments, Concordia University, Canada, 2016.
- [11] A. K. Gujba: PhD dissertation: Influence of Mechanical Surface Treatments on the Water Droplet Erosion Performance of Ti-6Al-4V, Concordia University, Canada, 2016.
- [12] F. G. Hammitt, F. J. Heymann: Liquid-erosion failures, failure analysis and prevention, *ASM Handbook*, ASM International, Vol. 11, 1986, pp. 163-171.
- [13] S. S. Cook: Erosion by Water-hammer, *Proceedings of the Royal Society of London. Series A*, Vol. 119, 1928, pp. 481-488.
- [14] F. J. Heymann: High- speed liquid impact between a liquid droplet and a solid surface, *Journal of Applied Physics*, Vol. 40, 1969, pp. 5113-5122.
- [15] J. E. Field: ELSI conference: Invited lecture. Liquid impact: Theory, experiment, applications, *Wear*, Vol. 233-235, 1999, pp. 1-12.
- [16] F. J. Heymann: On the Shock wave velocity and impact pressure in high-speed liquid-solid impact, *Journal of Basic Engineering*, Vol. 90, 1968, pp. 400-402.
- [17] M. B. Lesser: Analytic solution of liquid-drop impact problems, *Proceedings of the Royal Society of London. Series A*, Vol. 377, 1981, pp. 289-308.
- [18] J. H. Brunton: High speed liquid impact, *Proceedings of the Royal Society of London. Series A*, Vol. 260, 1966, pp. 79-85.

- [19] O. G. Engel: Mechanism of High-Speed-Waterdrop Erosion of Methyl Methacrylate Plastic, Journal of Research of the National Bureau of Standards, Vol. 54, Jan. 1955, pp. 51-59.
- [20] T. Sanada, K. Ando, T. Colonius: A Computational Study of High-Speed Droplet Impact, Tech Science Press, Vol. 7, No. 4, 2011, pp. 329-340.
- [21] M. J. Jackson, J. E. Field: Modelling liquid impact fracture thresholds in brittle materials, British Ceramic Transactions, Vol. 99, No. 1, 2000, pp. 1-13, doi: 10.1179/bct.2000.99.1.1.
- [22] F. J. Heymann: Erosion by liquids, Mechine Design, 1970, pp. 118-124.
- [23] D. C. Jenkins, J. C. Booker: The impingement of water drops on a surface moving at high speed. Proceedings of the Aerodynamic Capture of Particles, Leatherhead Surrey, UK, Jan. 1960; Pergamon Press: Oxford, UK, 1960.
- [24] M. E. Ibrahim, M. Medraj: Water Droplet Erosion of Wind Turbine Blades: Mechanics, Testing, Modeling and Future Perspectives, Materials, Vol. 13, No. 157, 2019, pp. 1-33, doi:10.3390/ma13010157.
- [25] F. J. Heymann: On the Time Dependence of the Rate of Erosion Due to Impingement or Cavitation, ASTM Special Technical Publication, Vol. 408, 1967, pp. 70-100.
- [26] J. E. Field, M. B. Lesser, J. P. Dear: Studies of two-dimensional liquid-wedge impact and their relevance to liquid-drop impact problems, Proceedings of the Royal Society of London. Series A, Mathematical and Physical Sciences, London, UK, 8th Oct. 1985, Vol. 401, No. 1821, pp. 225-249.
- [27] E. Honegger: Tests on erosion caused by jets, Brow Boveri Review, Vol. 14, 1927, pp. 95-104.

- [28] G73-10, ASTM, Standard test method for liquid impingement erosion using rotating apparatus. West Conshohocken, PA, USA: ASTM International, 2010.
- [29] F. J. Heymann: A survey of clues to relationship between erosion rate and impact parameters, In Second Meersburg Conference on Rain Erosion and Allied Phenomena, Bondensee, Federal German Republic, 1967.
- [30] I. Y. Oka, H. Miyata: Erosion behaviour of ceramic bulk and coating materials caused by water droplet impingement, *Wear*, Vol. 267, No. 11, 2009, pp. 1804-1810, doi: 10.1016/j.wear.2009.02.009.
- [31] M. Ahmad, M. Casey, N. Sürken: Experimental assessment of droplet impact erosion resistance of steam turbine blade materials, *Wear*, Vol. 267, No. 9-10, 2009, pp. 1605–1618, doi: 10.1016/j.wear.2009.06.012.
- [32] B. Lee, K. Riu, S. Shin, S. Kwon: Development of a water droplet erosion model for large steam turbine blades, *KSME International Journal*, Vol. 17, 2003, pp. 114-121.
- [33] F. J. Heymann: Liquid Impingement Erosion Wear, *ASM Handbook*, Materials Park, OH, USA, Vol. 18, 1992, pp. 221-223.
- [34] W. F. Adler: Particulate impact damage predictions, *Wear*, Vol. 186-187, Part 1(0), 1995, pp. 35-44.
- [35] K. Das, A. Hamed, D. Basu: Effect of Super-Cooled Water Droplet Characteristics on Fan Rotor-Ice Accretion, Published by the American Institute of Aeronautics and Astronautics, Inc., 2005, pp. 1-10.
- [36] W. Zhenlong: Drop "impact" on an airfoil surface, *Advances in colloid and interface science*, Vol. 256, 2018, pp. 23-47, doi: 10.1016/j.cis.2018.05.005.

- [37] M. Dina: Master thesis: Liquid Impingement Erosion Performance of Low Plasticity Burnished Ti6Al4V, Concordia University, Canada, 2014.
- [38] M. Ahmad: PhD dissertation: Experimental assessment of droplet impact erosion of low-pressure steam turbine blades, Institut für Thermische Strömungsmaschinen und Maschinenlaboratorium der Universität Stuttgart, Stuttgart (Germany), 2009.
- [39] P. Schmidt, G. Knauss: Impact resistance of liquids to non-use, Chemical Engineering and technology, Vol. 48, No. 7, 1976, pp. 659.
- [40] M. Rein: Phenomena of liquid drop impact on solid and liquid surfaces, Fluid Dynamics Research, Vol. 12, No. 2, 1993, pp. 61-93.
- [41] A. L. Gonor, V. Y. Yakovlev: Impact of a drop on a solid surface, Fluid Dynamics, Vol. 12, No. 5, 1977, pp. 767-771.
- [42] P. Savic, G. T. Boulton: The fluid flow associated with the impact of liquid drops with solid surfaces, Division of Mechanical Engineering, Vol, 29, 1955, pp. 1-15.
- [43] C. D. Stow, M. G. Hadfield: An experimental investigation of fluid flow resulting from the impact of a water drop with an unyielding dry surface, Proceedings of the Royal Society of London. Series A, Vol. 373, 1981, pp. 419-441.
- [44] R. Herring, K. Dyer, A. MacLeod, C. Ward: Computational fluid dynamics methodology for characterisation of leading edge erosion in whirling arm test rigs, Journal of Physics: Conference Series, Vol. 1222, 2019, pp. 1-11.
- [45] S. Sor, A. García-Magariño, A. Velazquez: Model to predict water droplet trajectories in the flow past an airfoil, Aerospace Science and Technology, Vol. 58, 2016, pp. 26-35, doi: 10.1016/j.ast.2016.07.015.

- [46] J. H. Brunton, Ed., *Erosion by Liquid Shock: Proceedings of the 2nd International Conference on Rain Erosion and Associated Phenomena*. RAE, Farnborough, England, 1967.
- [47] H. H. Shi, J. E. Field, C. S. J. Pickles: High Speed Liquid Impact Onto Wetted Solid Surfaces, *Journal of Fluids Engineering*, Vol. 116, 1994, pp. 345-348.
- [48] K. Fujisawa, T. Yamagata, N. Fujisawa: Damping effect on impact pressure from liquid droplet impingement on wet wall, *Annals of Nuclear Energy*, Vol, 121, 2018, pp. 260-268.
- [49] K. Fujisawa, T. Yamagata, N. Fujisawa: Liquid droplet impingement erosion on groove roughness, *Nuclear Engineering and Design*, Vol. 330, 2018, pp. 368-376.
- [50] H. Sasaki, N. Ochiai, Y. Iga: Numerical Analysis of Damping Effect of Liquid Film on Material in High Speed Liquid Droplet Impingement, *International Journal of Fluid Machinery and Systems*, Vol. 9, 2016, pp. 57-65.
- [51] J. Xiong, S. Koshizuka, M. Sakai: Investigation of Droplet Impingement onto Wet Walls Based on Simulation Using Particle Method, *Journal of Nuclear Science and Technology*, Vol. 48, 2011, pp. 145-153.
- [52] J. Banhart: Manufacturing routes for metallic foams, *Journal of Materials*, Vol. 52, No. 12, 2000, pp. 22-27.
- [53] J. Banhart: Foam Metal: The Recipe, *Europhysics News*, Vol. 30, No. 1, 1999, pp. 17-20.
- [54] A. M. Mostafid: PhD dissertation: Entrance and exit effects on flow through metallic foams, Master Thesis, Concordia University, Canada, 2007.

- [55] A. K. Flock, D. R. Guildenbecher, J. Chen, P. E. Sojka, H. J. Bauer: Experimental statistics of droplet trajectory and air flow during aerodynamic fragmentation of liquid drops, *International Journal of Multiphase Flow*, Vol. 47, 2012, pp. 37-49, doi: 10.1016/j.ijmultiphaseflow.2012.06.008.
- [56] M. H. Keegan, D. H. Nash, M. M. Stack: On erosion issues associated with the leading edge of wind turbine blades, *Journal of Physics D: Applied Physics*, Vol. 46, No. 38, 2013, pp. 1-20, 2013, doi: 10.1088/0022-3727/46/38/383001.
- [57] J. S. L. Mishnaevsky: Micromechanical model of surface erosion of polyurethane coatings on wind turbine blades, *Polymer Degradation and Stability*, Vol. 166, 2019, pp. 283-289, doi: 10.1016/j.polymdegradstab.2019.06.009.
- [58] H. S. Kirols: Master thesis: Water Droplet Erosion: Influencing Parameters, Representation and Comparisons, Concordia University, Canada, 2015.
- [59] A. L. N. Moreira, A. S. Moita, E. Cossali, M. Marengo, M. Santini: Secondary atomization of water and isooctane drops impinging on tilted heated surfaces, *Experiments in Fluids*, Vol. 43, 2007, pp. 297-313, doi: 10.1007/s00348-007-0330-2.
- [60] J. Hao, S. I. Green: Splash threshold of a droplet impacting a moving substrate, *Physics of Fluids*, Vol. 29, No. 1, 2017, pp. 1-9, doi: 10.1063/1.4972976.
- [61] A. K. Gujba, L. Hackel, D. Kevorkov, M. Medraj: Water droplet erosion behaviour of Ti–6Al–4V and mechanisms of material damage at the early and advanced stages, *Wear*, Vol. 359-359, 2016, pp. 109-122.

- [62] M. S. Mahdipoor, H. S. Kirols, D. Kevorkov, P. Jedrzejowski, M. Medraj: Influence of impact speed on water droplet erosion of TiAl compared with Ti6Al4V, Scientific reports, Vol. 5, 2015, pp. 1-18, doi: 10.1038/srep14182.
- [63] A. J. D. J. Dupuit: Etudes Theoriques et Pratiques Sur le Mouvement des aux dans les Canaux Decouverts les Terrains Permeables. Victor Dalmont, Paris, 1863.
- [64] X. Zhang, Y. Ling, Q. Gu: Extended Ergun equation of the flow resistance characteristics in porous graphitic foam, Materials Reports B, Vol. 26, No. 2, 2012, pp. 118-121.